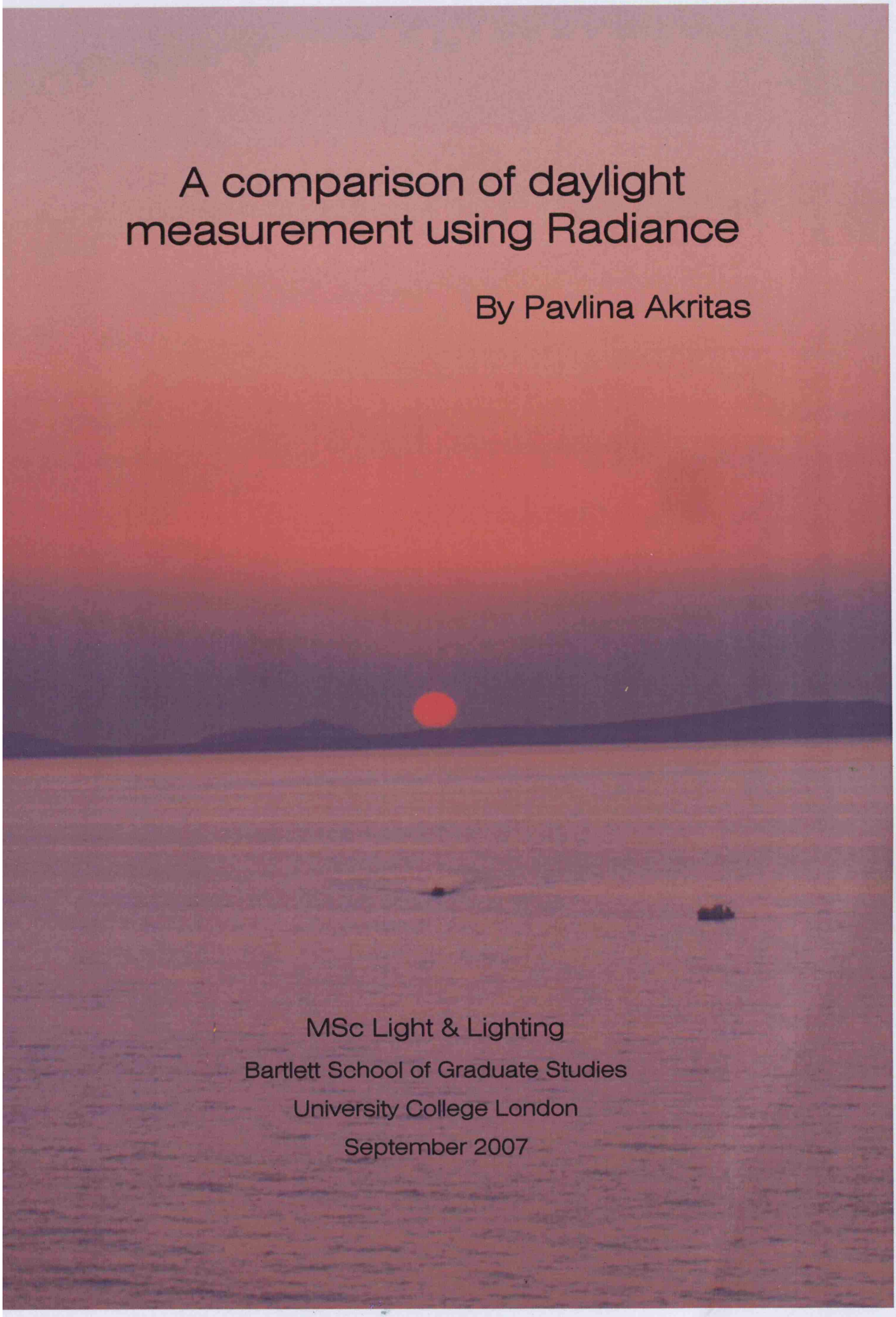

A comparison of daylight measurement using Radiance

By Pavlina Akritas

MSc Light & Lighting

Bartlett School of Graduate Studies

University College London

September 2007

ProQuest LLC
789 East Eisenhower Parkway
P.O. Box 1346
Ann Arbor, MI 48106-1346

Abstract

This dissertation compares the daylight coefficient approach for predicting time varying illuminance to a new method formulated by Peter J. Raynham based on the sunlight and daylight factors. The accuracy of the daylight coefficient derived illuminance predictions was verified by John Mardaljevic using the BRE-IDMP validation datasheet.

The prediction tool used for all the work described here is the *Radiance* lighting simulation system. Hourly predictions of daylight illuminance over a period of one year under variable sky and sun conditions were carried out for a full-size office space using both methods. The total annual klux-hours were then calculated, providing a simple metric to compare the two methods.

It has been demonstrated that Raynham's method and that of Mardaljevic diverge in terms of their results, with the difference becoming much more significant further away from the windows. It can therefore be deduced that Raynham's method can not be used to predict hourly internal illuminance levels.

Raynham's source of error is that he assumes an overcast sky to determine the diffuse component which has a dark horizon and brighter zenith with ratio of about 1 to 3. Thus, his method puts a lot of light higher in the sky as opposed to the ground as is the case of a clear sky.

It is impractical to also assume that the daylight coefficient approach is the ideal standard by which any potential method for predicting time varying illuminance should be compared against. The accuracy of this method is based on one set of results, and there are various sources of imprecision which could prove to be significant when the daylight coefficient approach is examined for a different locale.

Acknowledgements

The completion of this study would not have been possible without the generous help and support of a number of individuals to whom I am gratefully indebted.

Peter J. Raynham, my supervisor, not only for his guidance, commends and constructive suggestions, but also for proof-reading the final draft.

Chris Jackson, for his brief introduction to the *Radiance* lighting simulation system.

John Mardaljevic of the Institute of Energy and Sustainable Development at De Montfort University, for his previous research and unquestionable help.

Kevin Mansfield, the course director, for having me in the program.

Finally, I would like to express my gratitude to my family and friends for their constant support and motivation.

Table of Contents

Chapter 1

Introduction

"I can't define a space really as a space, unless I have natural light... natural light gives mood to space by nuances of light in the time of day and the season of the year as it enters and modifies the space"

-Louis Kahn

Daylight has not only important visual effects, but also important biological ones. These effects of daylight have been known and put to good use since ancient times, an example being heliotherapy, or the treatment of disease by exposure of the body to sun's rays[19]. Primarily, however, and throughout architectural history daylight has been used as a source of illumination. With the advent of the industrial revolution in the mid 18th century, daylight was competing with the various forms of artificial light as a means of illumination, up to the point where it appeared to be irrelevant[16]. After the oil embargo in 1973, there was a renewed interest in daylighting not only for energy conservation, but also because of the less tangible aspects of daylighting which relate more to the human spirit and the need for quality of life[16, 1].

Nowadays, daylight is mainly used as a replacement for artificial illumination. With the appropriate controls, daylight can provide considerable savings in energy, thus reducing carbon dioxide emissions and other greenhouse gases[14].

But daylighting involves much more than mere illumination; the changing nature of light, the spectral composition and the visual communication associated with windows are in many respects equally important[1]. Besides its effects on visual performance, daylight can also have a powerful influence on the atmosphere and visual impression gained of a space. In addition, humans depend on exposure to daylight to activate a wide range of physiological functions. The dynamic variation of daylight entrains the circadian rhythms of the body so as to coincide with the 24-hour

daily cycle. Circadian dysfunction can give rise to a condition known as seasonal affective disorder (SAD)[1]. Hence, the presence of daylight in buildings has a positive effect on the health and well-being of the occupants.

However, daylight can also adversely affect a human's wellbeing. For instance, there is growing awareness of the danger of exposure to ultraviolet light (UV), present in unfiltered daylight and particularly sunlight. Ultraviolet light is that part of the solar spectrum with a shorter wavelength than the visible waveband[1]. Having higher frequency, it has more energy, and as a consequence can have damaging effects on human beings. Overexposure to UV radiation can cause damage not only to the eyes, but also to skin cells, giving rise to reddening also called erythema, skin "ageing", and ultimately, skin cancer.

While there is growing awareness of the danger of overexposure to UV, the dangers of underexposure are often overlooked. Human evolution has occurred in the context of exposure to daylight, including UV[1]. Thus, human physiology depends on a certain degree to exposure to this lower part of the spectrum. The most important beneficial effect that UV has is the simulation of vitamin D production, without which calcium cannot be properly absorbed and utilised. For children, low vitamin D can result in rickets (bone deformation), while for the elderly there is a risk for bone brittleness, also known as osteoporosis [1].

When it comes to daylight, its harmful and beneficial effects are inextricably bound together. The intended purpose of daylighting systems is to improve the distribution and penetration of daylight into the room, increasing the usefulness of daylight while keeping its harmful effects to a minimum. As a consequence, a well daylit space needs both adequate lighting levels and light that is well distributed[5]. The specification of daylight requirements is covered in BS 8206 Part 2 and it is based on the daylight factor[2]. The daylight factor is defined as the ratio of internal to external illuminance and assumes a CIE standard overcast sky, irrespective of the prevailing climatic conditions for the locale of the proposed design[12]. However, under real skies the ratio of external to internal illuminance varies greatly[18]. Knowledge of the solar illuminance at a given location can have various applications related to the local architecture, energy savings in buildings, environmental policy and other fields where daylight estimation plays an important role[7].

As mentioned above, daylight is primarily used because of its contribution towards the efficient use of primary energy and increase in user's satisfaction.

Nevertheless, providing daylight in a building does not by itself lead to energy efficiency. Even a well daylit building may have a high level of lighting energy use if the lighting controls are inappropriate[10]. Studies have shown that poor acceptance of automatic systems can lead to the deactivation of lighting control systems[6]. Therefore, any control system used – whether in the form of shading devices such as light shelves, overhangs, and louvers, or daylight linked electric lighting controls – requires a careful building evaluation. A careful study of the plans related to energy efficient daylighting design will indicate where sufficient daylight is available, and where it will need to be supplemented[16].

A more accurate evaluation of daylight will take into account a full range of naturally occurring sky and sun conditions over a monitoring period of at least a year. This way the seasonal and short-term (if the time step is small enough) variations in daylight will be captured and the twin goals of energy efficiency and occupant comfort can be achieved.

To facilitate monitoring of sky and sun conditions, the IDMP was set up in 1991, by the Commission Internationale de l'Eclairage (International Lighting Commission) based in Vienna, Austria[17]. IDMP stands for International Daylight Measurement Programme (IDMP). There are 48 stations set up by the IDMP, specialised in high frequency and high quality daylight and solar radiation measurements. Of these 48 stations, 15 can also measure the distribution of light over the sky vault. The IDMP stations are of three classes based on the number of measurements they perform: basic, general and research. A major objective of the program was to collect long-duration time-series data for a range of daylight parameters including, at the stations designated "research class", measurement of the actual sky brightness distribution together with integrated quantities[13].

P. R. Tregenza and I.M. Waters were the first to attempt to set out a framework of calculations to give an overall view of the many stages of light diffusion from direct sunlight in the upper atmosphere to inter-reflections within a room[18]. Their solution was based on the daylight coefficient approach. The daylight coefficient approach requires that the sky be broken into many patches. The internal illuminance at a point that results from a patch of known luminance sky can then be computed, and thus the internal illuminance for arbitrary sky / sun conditions can be determined using relatively simple arithmetic operations on matrices[11].

The accuracy of the daylight coefficient derived illuminance predictions was verified through *Radiance* by John Mardaljevic of De Montfort University (Leicester) using the BRE-IDMP validation datasheet[11]. *Radiance* uses a backward, hybrid deterministic-stochastic ray-tracing algorithm, and allows the modelling of three-dimensional environments of arbitrary shape using a detailed description of the material's optical properties. Validation studies have demonstrated that the *Radiance* system has the potential to accurately predict daylight illumination levels for a wide range of naturally occurring sky conditions[11].

However, measured sky brightness data is very limited at this point in time[11]. Therefore, a theoretical model to generate a sky luminance distribution is used instead. Most sky models are devised to be applicable to only a limited range of possible sky conditions, namely overcast and clear. However, these extreme sky types are only important for window design; for energy simulation these do not fully represent conditions occurring in reality[4]. The Perez model was specifically formulated to represent all (or at least the majority) of naturally occurring sky conditions[11]. Wider application of the "narrow-range" models is also possible by blending the luminance patterns of two or more skies in response to meteorological conditions. Most commonly, an overcast luminance pattern is combined with one or more non-overcast patterns[9]. Predictions of internal illuminance using sky models and sky model blends where compared against those using measured sky luminance patterns. The luminance predictions of the Perez model and the sky model blends performed comparably well, although not as well as the luminance predictions using measured skies[11].

Luminance distributions, which model the sky under a wide range of conditions from heavily overcast sky to cloudless weather, have become available with the work done by Kittler, Perez, and Darula[3]. In their work, the relative sky luminance distribution and sky parameterisation of fifteen standardised patterns is described. These have been published in BS ISO 15469:2004 and are considered to be a universal basis for the classification of measured sky luminance distributions.

Chapter 2

Protocol of study

This paper compares the daylight coefficient approach for daylight analysis to a new method formulated by Peter J. Raynham of the Bartlett School of Graduate Studies at UCL (London).

Raynham has developed a new method in an attempt to accurately predict solar illuminances. His method involves determining the daylight and sunlight factors, and combining the two to determine true daylighting performance. The sunlight factor, unlike the daylight factor, describes the ratio of internal illuminance at a point to the global horizontal illuminance due to the light direct from the sun. Not only is it simpler, but this method has the advantage (over the daylight coefficient approach) that it allows for a more complex analysis of illumination.

The study was carried out entirely through the use of computer simulations within the *Radiance* lighting simulation system. A simple office building, assumed to be in London (UK) at latitude of 51.5° N and a longitude of 0°, has been modelled. The UK "research class" station whose long-duration time-series data was used, was at the Building Research Establishment (BRE) in Garston (UK). The station is located at a latitude of 51.7° N and a longitude of 0.37° W and the measurements for a range of daylight parameters were taken during 1992.

Hourly predictions of daylight illuminance over a period of one year under variable sky and sun conditions were carried out and the total annual klux-hours were calculated, providing a simple metric to compare the two methods. A month-hour sky analysis furnishes the following useful information[7]:

i. Knowledge of the extreme (minimum and maximum) values of the month-hour illuminance distribution, which is valuable for architects and building designers in determining building openings.

ii. These extreme values, which are also useful for energy-saving calculations in buildings, support the recommendations of building codes for daylight

distribution in rooms.

iii. The gradation between minimum and maximum illuminance values, which is useful because it yields knowledge about the rate of change in the levels between the two extremes.

Chapter 3

Methodology

This chapter is accompanied by the attached CD-ROM. All files can be found under the corresponding chapter.

3.1 Preparation

3.1.1 The office model

A simple 3D model of an office building was constructed using *Radiance*'s own scripts and surface generators. The office was assumed to be located in London at a latitude of 51.5°. The office was 18m wide and 25.4m deep and had a floor to ceiling height of 2.7m (Figures 3.1 and 3.2).

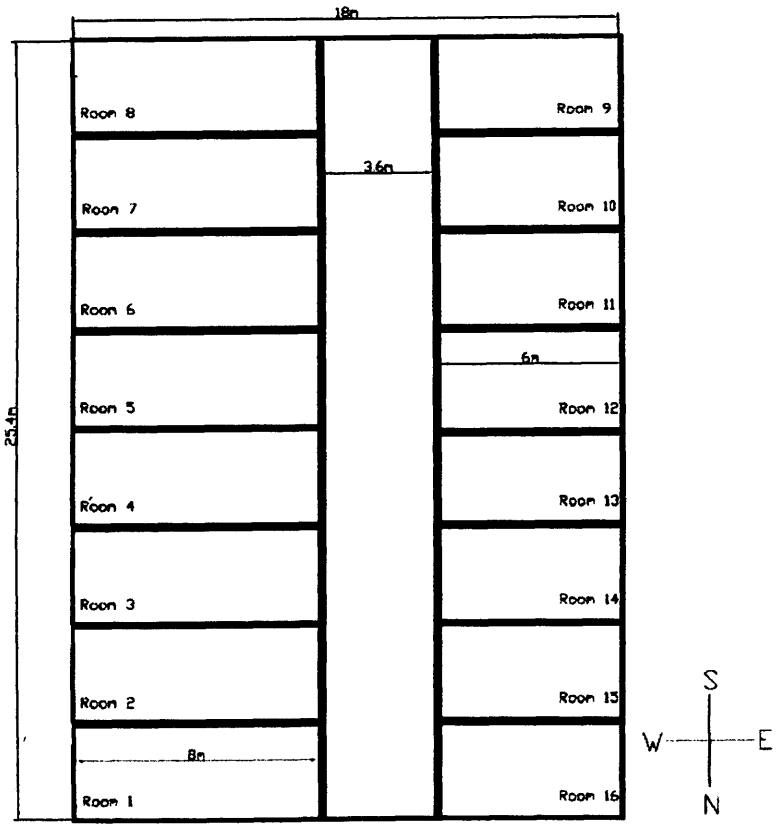

Figure 3.1: Office plan

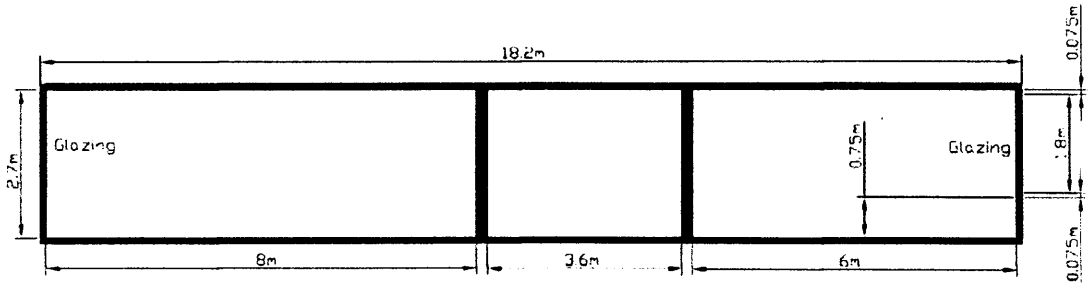

Figure 3.2: Office section

There were two different sized rooms in the building. The first one was 3m wide and 8m deep with west-facing glazing, and the second one was 3m wide and 6m deep with east-facing glazing. These were separated by a 3.6m deep corridor. The walls separating the rooms were 0.2m thick. Each room had one window which was 3m wide and 2m high and 0.75m from the floor. The rooms were left unfurnished and the surface reflectances were chosen to correspond to a typical office.

Two **rad** programs were written controlling the window and scene compilation (win.rad and office.rad). The glazing of the window was of size 2.85m by 1.8m and was made of a neutral body tint `glass` with a transmittance, (T_n), of 0.65. In *Radiance*, however, it is the transmissivity, (t_n), of the material that is specified:

$$t_n = \frac{\left(\sqrt{0.8402528435 + 0.0072522239 \times T_n^2} - 0.9166530661\right)}{0.0036261119 \times T_n} \qquad (3\text{-}1)$$

Thus,

$$t_n = \frac{\left(\sqrt{0.8402528435 + 0.0072522239 \times \left(0.65^2\right)} - 0.9166530661\right)}{0.0036261119 \times 0.65} = 0.709748$$

Both the window panes and frames were constructed with 4-sided planar `polygons`. The width of the bars was set to 0.075m. The frames were made of grey `plastic` and had a diffuse reflectance of 0.7. The specularity and roughness were set to 0.01.

```
% win.rad
# glazing material
void glass glass1
0
0
3 0.709748 0.709748 0.709748

# frame      ,
void plastic frame
0
0
5 0.7 0.7 0.7 0.01 0.01
```

```
% win.rad cont.
frame polygon bot
0
0
12      0       0       0
        3.0     0       0
        3.0     0       0.075
        0       0       0.075
frame polygon top
0
0
12      0       0       2
        3.0     0       2
        3.0     0       1.875
        0       0       1.875
frame polygon left
0
0
12      0       0       0
        0.075   0       0
        0.075   0       2
        0       0       2

frame polygon right
0
0
12      3.0     0       0
        2.925   0       0
        2.925   0       2
        3.0     0       2

# window pane
glass1 polygon win
0
0
12      0.075   0  0.075
        2.925   0  0.075
        2.925   0  1.875
        0.075   0  1.875
```

The windows were `xformed` into office.rad. This allowed to easily create an array of repeated objects. The building was specified to begin at the XYZ co-ordinates of (0 0 0). The floor, ceiling and exterior walls were made of `plastic` with reflectivities of 0.2, 0.7, and 0.5, respectively. Each was constructed using a 4-sided planar `polygon`, and were assumed to be matte and polished, thus the specularity and roughness were set to 0. The internal walls were also made of `plastic` with a reflectivity of 0.5. However, these were constructed using the `genbox` command, which created a parallelepiped with sharp corners.

```
% office.rad

#floor
void plastic floor
0
0
5     0.2   0.2   0.2   0          0
#      r     g     b  specularity  roughness

floor polygon f1
0
0
12    0     0     0
      18    0     0
      18    25.4  0
      0     25.4  0
```

```
% office.rad cont.
# exterior walls
void  plastic wall
0
0
5     0.5   0.5   0.5   0     0

wall polygon wall1
0
0
12    0     0     0
      18    0     0
      18    0     2.705
      0     0     2.705

wall polygon wall2
0
0
12    18    0     0
      18    25.4  0
      18    25.4  0.75
      18    0     0.75

wall polygon wall3
0
0
12    18    25.4  0
       0    25.4  0
       0    25.4  2.705
      18    25.4  2.705

wall polygon wall4
0
0
12     0    25.4  0
       0     0    0
       0     0    0.75
       0   25.4   0.75

#these are the windows being xformed into the stored

!xform      -e    -n    w1    -rz   90.00  -t   0     0     0.75  win.rad
!xform      -e    -n    w2    -rz   90.00  -t   0     3.2   0.75  win.rad
!xform      -e    -n    w3    -rz   90.00  -t   0     6.4   0.75  win.rad
!xform      -e    -n    w4    -rz   90.00  -t   0     9.6   0.75  win.rad
!xform      -e    -n    w5    -rz   90.00  -t   0     12.8  0.75  win.rad
!xform      -e    -n    w6    -rz   90.00  -t   0     16    0.75  win.rad
!xform      -e    -n    w7    -rz   90.00  -t   0     19.2  0.75  win.rad
!xform      -e    -n    w8    -rz   90.00  -t   0     22.4  0.75  win.rad
!xform      -e    -n    w9    -rz   90.00  -t   18    0     0.75  win.rad
!xform      -e    -n    w10   -rz   90.00  -t   18    3.2   0.75  win.rad
!xform      -e    -n    w11   -rz   90.00  -t   18    6.4   0.75  win.rad
!xform      -e    -n    w12   -rz   90.00  -t   18    9.6   0.75  win.rad
!xform      -e    -n    w13   -rz   90.00  -t   18    12.8  0.75  win.rad
!xform      -e    -n    w14   -rz   90.00  -t   18    16    0.75  win.rad
!xform      -e    -n    w15   -rz   90.00  -t   18    19.2  0.75  win.rad
!xform      -e    -n    w16   -rz   90.00  -t   18    22.4  0.75  win.rad

# ceiling
void plastic ceiling
0
0
5     0.7   0.7   0.7 0 0

ceiling polygon ceil1
0
0
12    0     0     2.7
      18    0     2.7
      18    25.4  2.7
      0     25.4  2.7

# walls of rooms
void plastic iwall
0
0
5     0.5   0.5   0.5   0     0
```

```
% office.rad cont.

!genbox iwall iw1 8 0.2 2.705 | xform   -t   0  3    0
!genbox iwall iw2 8 0.2 2.705 | xform   -t   0  6.2  0
!genbox iwall iw3 8 0.2 2.705 | xform   -t   0  9.4  0
!genbox iwall iw4 8 0.2 2.705 | xform   -t   0  12.6 0
!genbox iwall iw5 8 0.2 2.705 | xform   -t   0  15.8 0
!genbox iwall iw6 8 0.2 2.705 | xform   -t   0  19   0
!genbox iwall iw7 8 0.2 2.705 | xform   -t   0  22.2 0

!genbox iwall iw8 6 0.2 2.705 | xform   -t   12  3   0
!genbox iwall iw9 6 0.2 2.705 | xform   -t   12 6.2  0
!genbox iwall iw10 6 0.2 2.705 | xform  -t   12 9.4  0
!genbox iwall iw11 6 0.2 2.705 | xform  -t   12 12.6 0
!genbox iwall iw12 6 0.2 2.705 | xform  -t   12 15.8 0
!genbox iwall iw13 6 0.2 2.705 | xform  -t   12 19   0
!genbox iwall iw14 6 0.2 2.705 | xform  -t   12 22.2 0

# walls of central corridor

!genbox iwall iw15 0.2 25.4 2.705 | xform  -t  8  0 0
!genbox iwall iw16 0.2 25.4 2.705 | xform  -t 11.8 0 0

#table

#void plastic brown_paint
0
0
5     0.4   0.25  0.05  0.05  0.03

# a brown table in room 1
!genbox brown_paint table_top1 1 0.5 0.04 | xform   -t  0.5  2  0.86
!genbox brown_paint table_left_top_leg1 0.04 0.04 0.86 | xform  -t 0.54 2.46  0
!genbox brown_paint table_left_bottom_leg1 0.04 0.04 0.86 | xform -t 0.54 2.04 0
!genbox brown_paint table_right_top_leg1 0.04 0.04 0.86 | xform  -t 1.42 2.46 0
!genbox brown_paint table_right_bottom_leg1 0.04 0.04 0.86 | xform -t 1.42 2.04 0

# a brown table in room 11
!genbox brown_paint table_top11 1 0.5 0.04 | xform   -t 16.5 8.4 0.86
!genbox brown_paint table_left_top_leg11 0.04 0.04 0.86 | xform  -t 16.54 8.82 0
!genbox brown_paint table_left_bottom_leg11 0.04 0.04 0.86 | xform  -t 16.54 8.44 0
!genbox brown_paint table_right_top_leg11 0.04 0.04 0.86 | xform  -t 17.42 8.82 0
!genbox brown_paint table_right_bottom_leg11 0.04 0.04 0.86 | xform -t 17.42 8.44  0

# a red ball
void plastic red_plastic
0
0
5     .7    .05   .05   .05   .05

# a sphere on top of table 1
red_plastic sphere ball1
0
0
4     1     2.25  1.025 0.125

# a sphere on top of table 11

red_plastic sphere ball11
0
0
4     17    8.65  1.025 0.125
```

For viewing purposes two tables with a ball on top were also compiled in rooms 1 and 11. The tables were made of a brown coloured `plastic` with RGB values of 0.4, 0.25, and 0.05. The specularity and roughness were set to 0.05 and 0.03. Each table was constructed using the `genbox` command five times. The balls were made of red `plastic` with RGB values of 0.7, 0.05 and 0.05, and the specularity and

roughness were both set to 0.05. Each ball was defined as a `sphere` with a radius of 0.125m.

Once all the geometry has been assembled and appropriately located, the materials and geometry were converted into an octree using the `oconv` command.

```
% RADoffice.oct
oconv -f office.rad > RADoffice.oct
```

3.1.2 Calculation points

The calculation points lay on the work-plane (0.7m from the floor) along a straight line from the windows to the back of each room (Figures 3.3, 3.4, 3.5, 3.6 and 3.7).

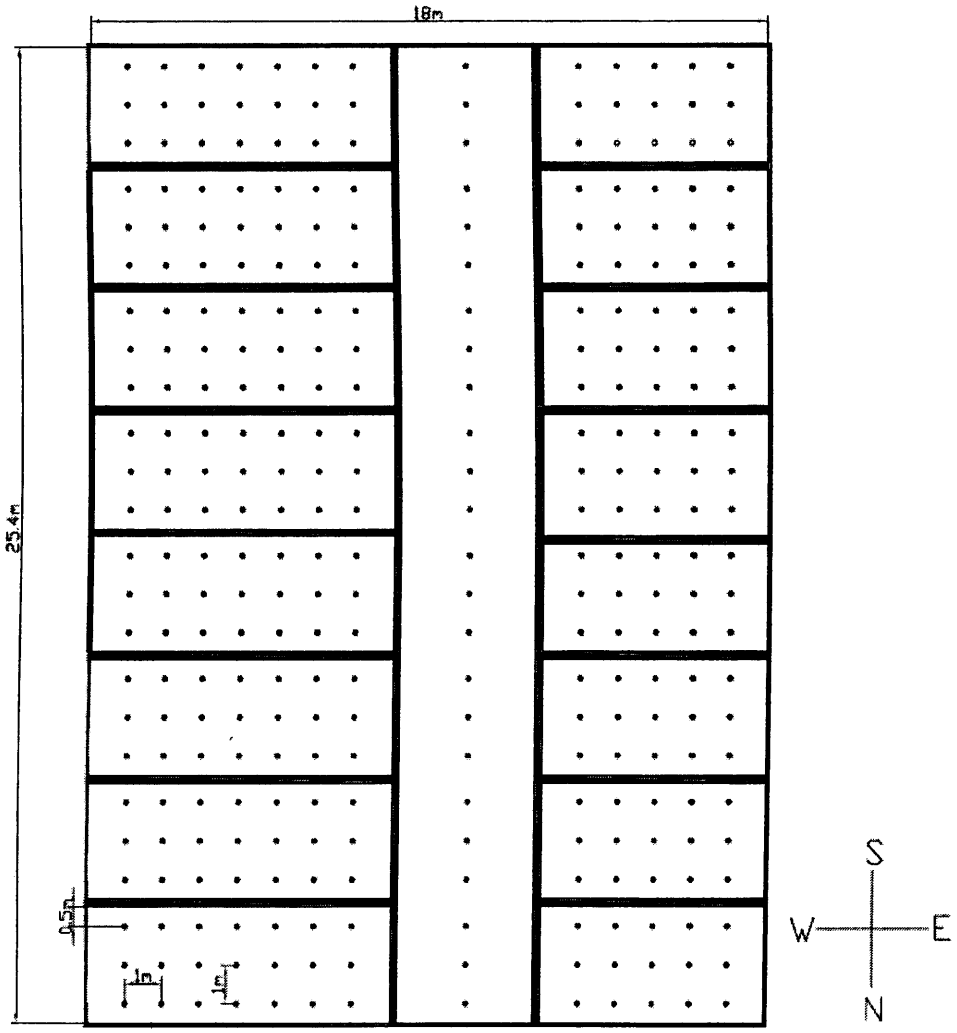

Figure 3.3: Calculation points location plan

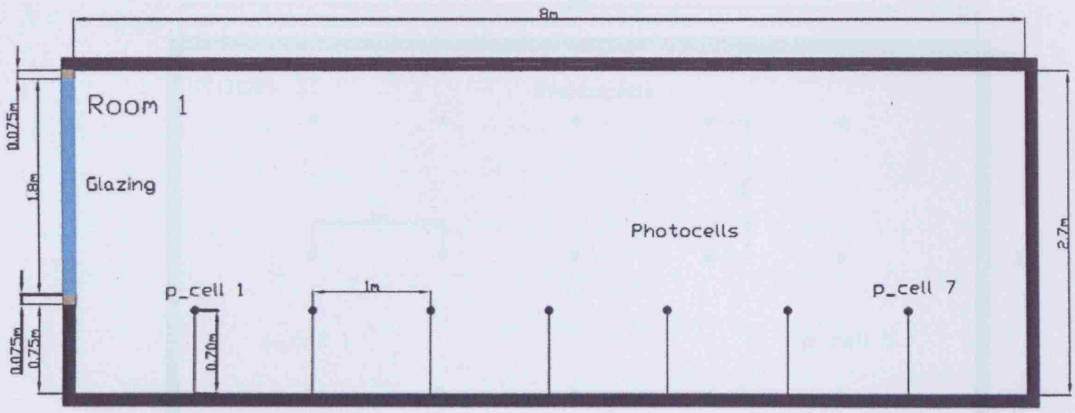

Figure 3.4: Calculation points location Room 1 section

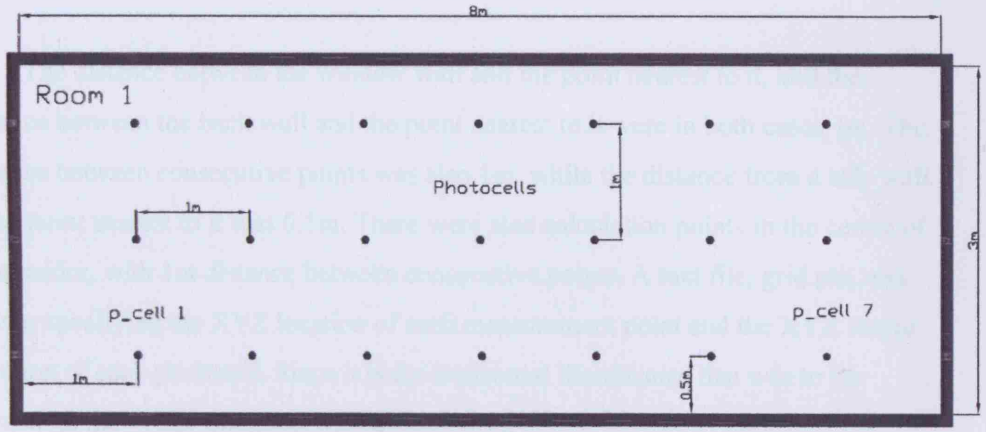

Figure 3.5: Calculation points location Room 1 plan

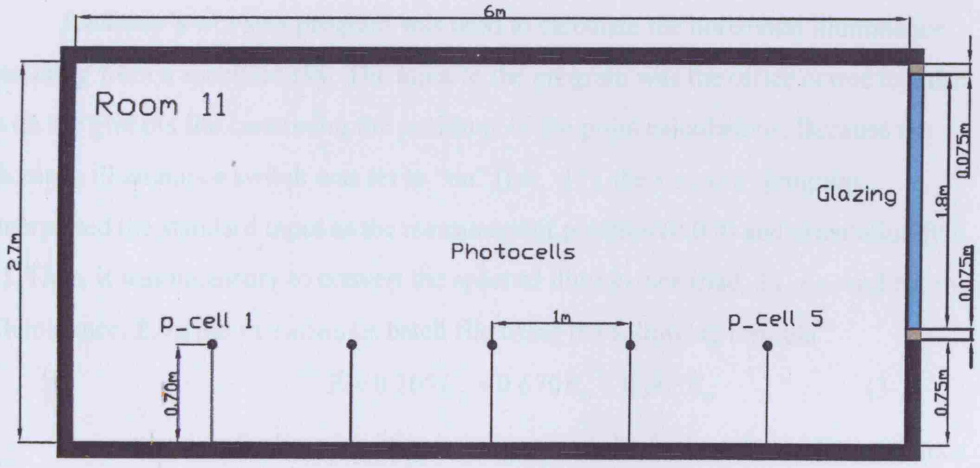

Figure 3.6: Calculation points location Room 11 section

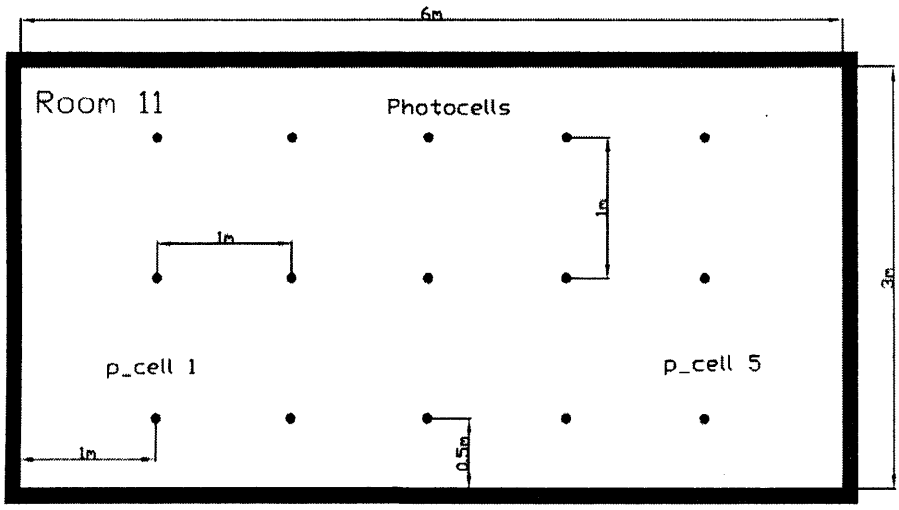

Figure 3.7: Calculation points location Room 11 plan

The distance between the window wall and the point nearest to it, and the distance between the back wall and the point nearest to it were in both cases 1m. The distance between consecutive points was also 1m, while the distance from a side wall to the point nearest to it was 0.5m. There were also calculation points in the centre of the corridor, with 1m distance between consecutive points. A text file, grid.pts, was written specifying the XYZ location of each measurement point and the XYZ vector direction of each photocell. Since it is the horizontal illuminance that was to be calculated, the vector direction was set to (0 0 1).

3.1.3 Data collection

Radiance's `rtrace` program was used to calculate the horizontal illuminance resulting from a specified sky. The input to the program was the office octree together with the grid.pts file containing the positions of the point calculations. Because the Boolean illuminance switch was set to "on" (i.e., -I+), the `rtrace` program interpreted the standard input as the measurement position (0 0 0) and orientation (0 0 1). Thus, it was necessary to convert the spectral illuminance triad, E_R, E_G, and E_B, to illuminance, E, in the `rtracesim` batch file using the following formula[8]:

$$E = 0.265E_R + 0.670E_G + 0.065E_B \qquad (3\text{-}2)$$

The output was further piped through `rcalc` to obtain the achromatic irradiance directly.

3.1.4 Selecting the ambient parameters values

The accuracy of the illuminance calculations is highly dependent on the setting of the ambient parameters in the `rtrace` program which control the depth (i.e. number of reflections) and resolution of the inter-reflection calculation[11]. The computation cost of an illuminance calculation is very sensitive to the setting of these key ambient parameters[11]. Since hundreds of lighting simulations were to be carried out, it was necessary to keep the computation time relatively low without jeopardising the accuracy of the results. Thus, a parameter optimisation study was carried out where the sensitivity of the accuracy and the simulation time to variation in six ambient parameters was investigated under a 10,000lux overcast sky. These parameters were the number of ambient bounces, the ambient accuracy, the ambient resolution, the number of ambient divisions, the number of ambient supersamples and the constant ambient approximation.

Initially, the number of ambient bounces (ab) was varied, since this is the most important of the ambient calculation parameters. For the study the number of ambient bounces was varied between 1, 2, 3, 4, 5, 6, and 8 (Figure 3.8).

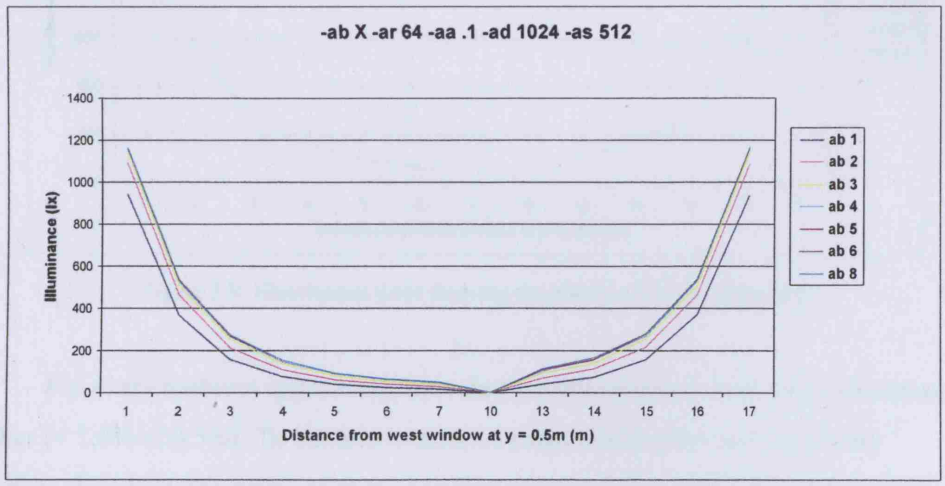

Figure 3.8: Illuminance plots showing the effects of the –ab parameter

Further away from the windows, the illuminance predictions for all ambient bounces were relatively similar. However, close to the windows the predictions agreed less. The illuminance values at 6 ambient bounces were very close to the illuminance values at 8 ambient bounces (<1.5% at 0.5m). Thus, the ambient bounces in the `rtrace` program were set to 6, in order to accurately calculate the indirect illumination while decreasing the computation time (Table 3.1).

-ab	Computation time
1	>1 min
2	2min
3	7min
4	9min
5	10min
6	11min
8	17min

Table 3.1: Computation time for a range of ab settings

The next parameter that was varied was the ambient approximation (aa). Illuminances were collected with the ambient approximation set to 0.05, 0.1, 0.15 and 0.2 (Figure 3.9).

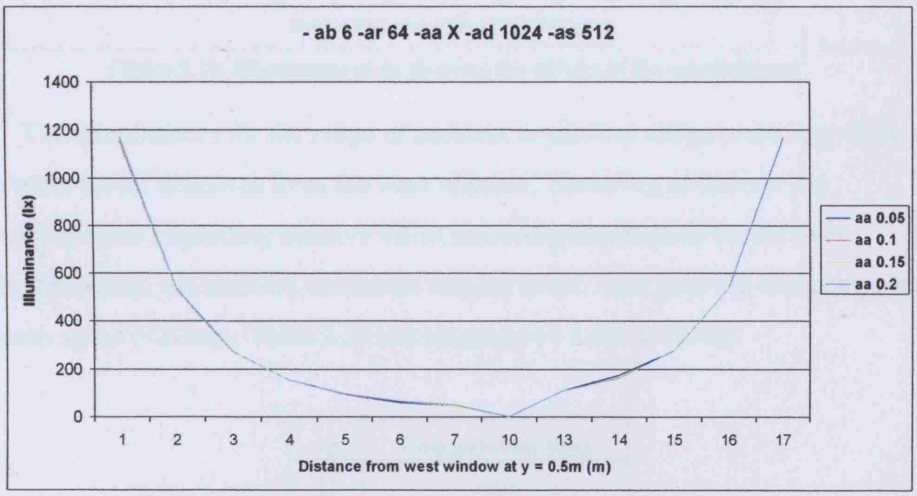

Figure 3.9: Illuminance plots showing the effects of the –aa parameter

For every ambient approximation value the illuminances were very close to each other (< 1.0% at 0.5m). To be able to achieve exact shading for each and every surface, however, the ambient approximation was set to 0.1. The computation time was also kept relative low (<10min; Table 3.2).

-aa	Computation time
0.05	50min
0.1	10min
0.15	4min
0.2	2min

Table 3.2: Computation time for a range of –aa settings

Having settled on a value for the ambient approximation, the illuminance was evaluated for a range of ambient resolution (ar) values. The range consisted of the ambient resolution being equal to 32, 64 or 128 (Figure 3.10).

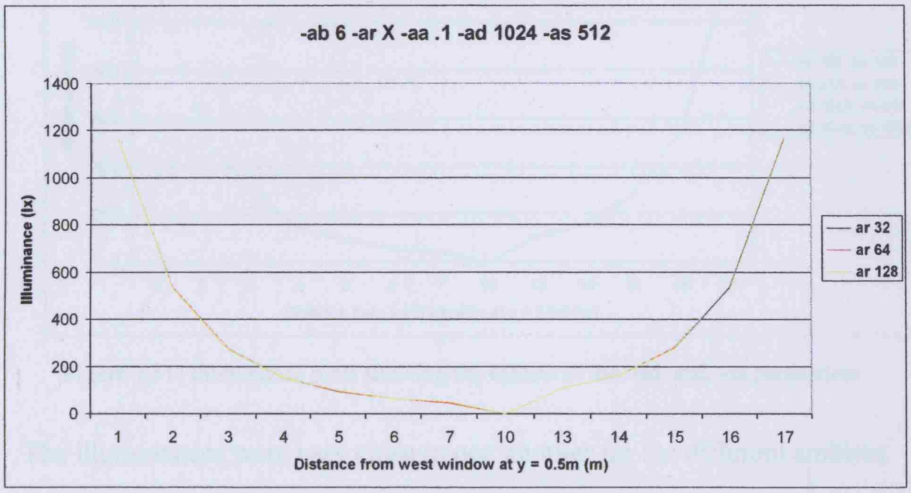

Figure 3.10: Illuminance plots showing the effects of the –ar parameter

The illuminances for the range of ambient resolution values were very close to each other for all distances from the west window. However, to prevent the calculation from expending massive effort resolving illuminance values over negligible scales, the ambient resolution was set to 64. This gave the best compromise between speed (<12min; Table 3.3) and accuracy (< 1.6% at 0.5m).

-ar	Computation time
32	7min
64	12min
128	17min

Table 3.3: Computation time for a range of –ar settings

Next, the ambient divisions (ad) and the ambient supersamplings (as) were varied. The ambient divisions were varied between 256, 512, 1024, and 2048. At each ambient division value, the ambient supersampling value was set to one half of the corresponding ambient division value (Figure 3.11, see next page).

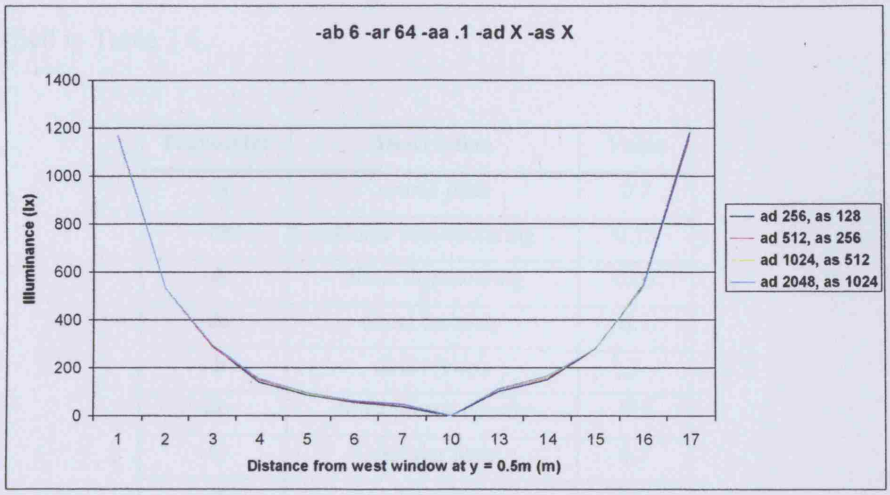

Figure 3.11: Illuminance plots showing the effects of the –ad and –as parameters

The illuminances were very close to one another for the different ambient division and ambient supersampling values. However, the sun patches on the surfaces of each room could be significant sources of indirect illumination. Thus, in order to capture these potential sources, the number of ambient divisions was set to 1024 and the number of ambient supersamplings was set to 512. The computation time was also kept relatively low (<10min; Table 3.4).

-ad	-as	Computation time
256	128	2min
512	256	5min
1024	512	10min
2048	1024	22min

Table 3.4: Computation time for a range of –ad and –as settings

The constant ambient value (av) was set to zero as absolute accuracy was required for illuminance prediction.

The parameters that were determined using the parameter optimisation study are listed in Table 3.5.

Parameter	Value
-ab	6
-aa	0.10
-ar	64
-ad	1024
-as	512
-av	0

Table 3.5: Parameter values

For reasonably accurate rendering, the rest of the `rtrace` parameters were set as specified in Table 3.6.

Parameter	Description	Value
-dj	source jitter	0.7
-ds	source substructuring	0.15
-dt	direct thresholding	0.05
-dc	direct certainty	0.5
-dr	direct relays	3
-dp	direct pretest density	512
-sj	specular jitter	0.7
-st	specular threshold	0.15
-lr	limit reflection	8
-lw	limit weight	0.002

Table 3.6: Additional parameter values

With this parameters combination, each simulation took approximately 22 minutes to complete.

3.1.5 Lighting visualisation

The `rpict` rendering program was used to produce the highest-quality pictures for rooms 1 (Figure 3.12) and 11 (Figure 3.13) under the standard 10,000 lux CIE overcast sky. The program created an image taken from a virtual camera located and oriented as specified by the viewing position (vp) and viewing direction (vd) parameters. The output of the `rpict` program was further passed through `pfilt` for exposure adjustment and antialiasing. For room 1:

```
% rpicktest_1

# room 1 picure
rpict -t 5 -vp 4 0.5 1.5 -vd -1 1 0  -ab 6 -aa 0.1 -ad 1024 -as 512 -ar 64 -dj .7 -ds .15 -dt
.05 -dc .5 -dr 3 -dp 512 -sj .7 -st .15 -lr 8 -lw .002 -x 2048 -y 1536 -vh 89 -vv 65
ciesky.oct > ciesky.pic
pfilt -x /2 -y /2 -r 1 ciesky.pic > cieskyf.pic
ra_tiff -e -1 cieskyf.pic room_1.tif
```

And room 11:

```
% rpicktest_11

# room 11 picure
rpict -t 5 -vp 13 7 1.5 -vd -1 1 0  -ab 6 -aa 0.1 -ad 1024 -as 512 -ar 64 -dj .7 -ds .15 -dt
.05 -dc .5 -dr 3 -dp 512 -sj .7 -st .15 -lr 8 -lw .002 -x 2048 -y 1536 -vh 89 -vv 65
ciesky.oct > ciesky.pic
pfilt -x /2 -y /2 -r 1 ciesky.pic > cieskyf.pic
ra_tiff -e -1 cieskyf.pic room_11.tif
```

Figure 3.12: Room 1

Figure 3.13: Room 11

3.2 Determining daylight illuminance using Mardaljevic's method

3.2.1 Fundamentals

Daylight that falls on a surface in a room depends on the luminance of the sky and the form and materials of the surrounding surfaces[18]. The two factors are, for most practical purposes, independent of each other. Although the factor due to the built form can be taken to be constant, the sky luminance can vary independently from one angle of view to another. It is necessary, therefore, to break the sky into many patches. Each patch is analysed, and the total illuminance for an arbitrary sky luminance distribution is determined by summing all these components.

The illuminance, $\Delta E_{\gamma\alpha}$, produced at a point in a room from a small patch of sky at altitude, γ, and azimuth, α, is defined as:

$$\Delta E_{\gamma\alpha} = D_{\gamma\alpha} \times L_{\gamma\alpha} \Delta S_{\gamma\alpha} \qquad (3\text{-}3)$$

where $L_{\gamma\alpha}$ is the luminance of the element of sky and $\Delta S_{\gamma\alpha}$ is the solid angle of the patch of sky. $D_{\gamma\alpha}$ is defined as the "daylight coefficient" and depends on the physical characteristics of the room and the external environment such as the room geometry, surface reflectances, window transmittance, outside obstructions and reflections, Figure 3.14[6].

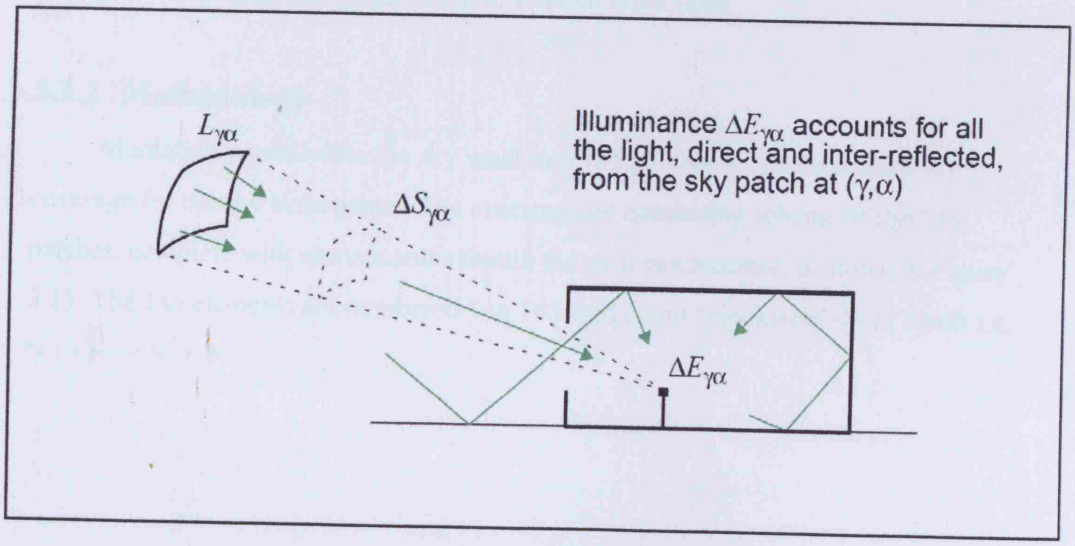

Figure 3.14: Daylight coefficient basics

The total illuminance, E, produced at a point in a room is then obtained from[18]:

$$E = \int_0^{2\pi} \int_0^{\pi/2} D_{\gamma\alpha} L_{\gamma\alpha} \cos\gamma d\gamma d\alpha \qquad (3\text{-}4)$$

Usually, some form of finite-element calculation is required for even the simplest realistic scene[11].

If the sky and external surfaces are divided into n finite angular zones, then equation 3-4 can be written in the form[18]:

$$E = \sum_{p=1}^{n} D_p S_p L_p \qquad (3\text{-}5)$$

Equation 3-5 considers only one point in a room, for which the daylight coefficients may be considered as a vector $[D_1\ D_2 \ldots\ D_n]$ [12]. Dividing the internal surfaces of the room into m finite areas, then the array of coefficients becomes an $m \times n$ matrix, $\overline{D}$. The illuminances, $E_1, E_2, \ldots, E_m$, can then be described by the column vector $\overline{E}$ containing m elements. Similarly, another column vector, $\bar{c}$, can be formed from the n products of angular size and luminance. This gives the compact matrix formulation[12]:

$$\overline{E} = \overline{D} \times \bar{c} \qquad (3\text{-}6)$$

The daylight coefficient matrix can itself be expressed as the product of three matrices[18]:

$$D = R_3 \times R_2 \times R_1 \qquad (3\text{-}7)$$

where R_1 defines the external obstruction to light, R_2 the direct component of the daylight coefficients, and R_3 the result of internal reflections.

3.2.2 Methodology

Mardaljevic subdivides the sky vault into 145 patches to give complete sky coverage for the sky hemisphere. The ordering and numbering scheme of the 145 patches, complete with altitude and azimuth for each patch centre, is shown in Figure 3.15. The 145 elements are numbered 1 to 145, and count "clockwise" from North i.e. N → E → S → W[11].

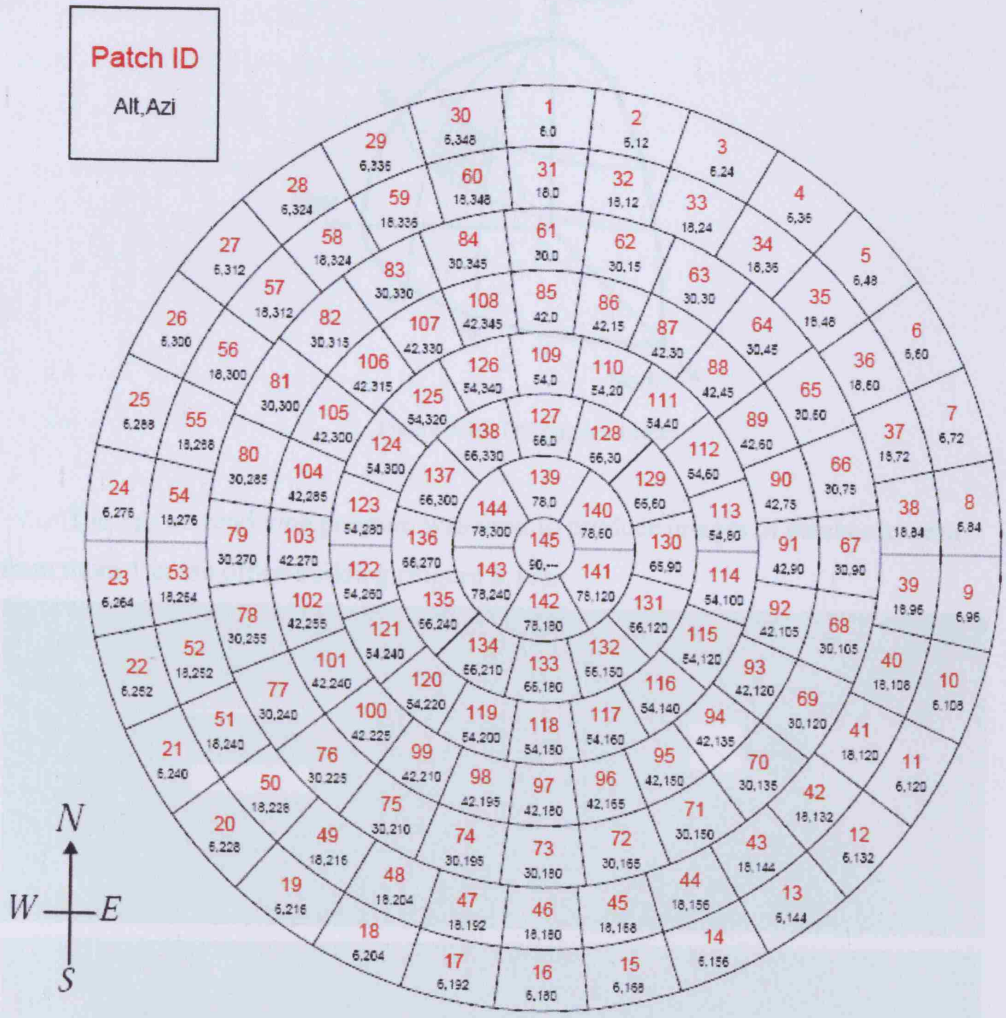

Figure 3.15: Patch identification

However, *Radiance* only samples light sources using a single ray to the source centre. This could give rise to errors where the source is partially occluded from a point within the room and the value of illuminance at that point will only depend on whether there is direct unobstructed line from the point to the centre of the source. To remove this potential source of error, each patch was further sub-divided into smaller 1° "circular" patches, allowing each of the 145 patches to be sampled with multiple rays rather than one (Figure 3.16). Thus, a total of 19,582 1° patches were sampled. The exact location in terms of altitude and azimuth of each of the 19,582 patches was written in the XYZ_vector_of_patches.xls file.

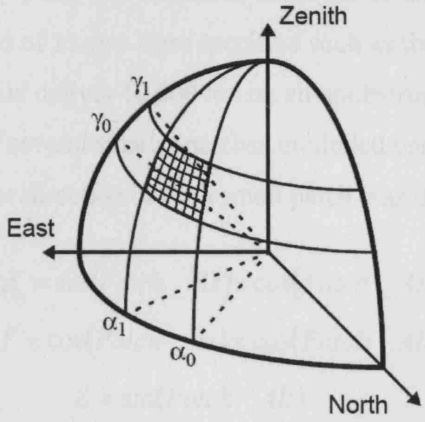

Figure 3.16: DC patch schemes

The `rpict` rendering program was used to produce images of patches as seen from room 1 in the office building (Figure 3.17).

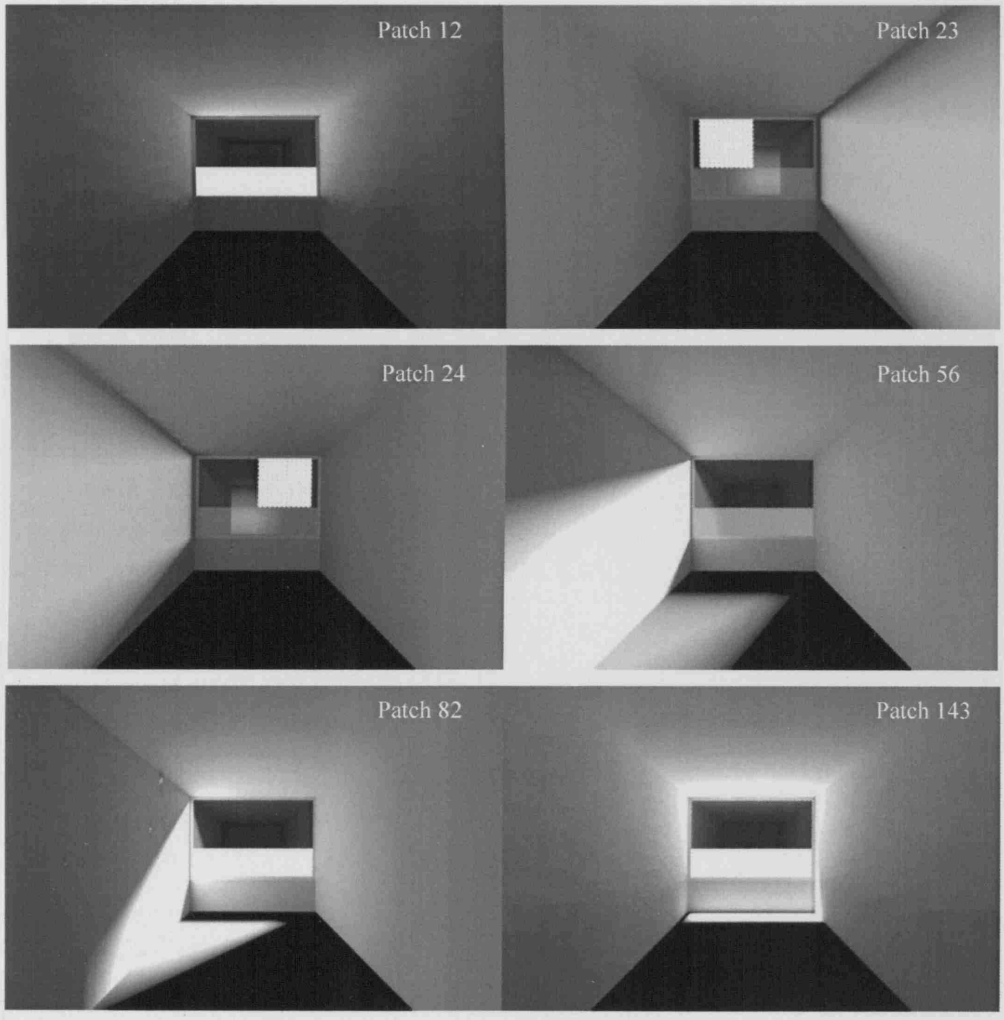

Figure 3.17: Images of patches in room 1

Each luminous sky patch was modelled in *Radiance* using a source angle type `light`. The RGB values of `light` were specified such as the central patch of the sub-divided 145th patch would deliver 10,000 lux on an unobstructed horizontal surface. Each patch consisted of several smaller patches modelled using a geometric type `source`. The *XYZ* vector direction of each small patch was determined as follows:

$$X = \sin(Patch\_Az) \times \cos(Patch\_Alt) \quad (3\text{-}8)$$

$$Y = \cos(Patch\_Az) \times \cos(Patch\_Alt) \quad (3\text{-}9)$$

$$Z = \sin(Patch\_Alt) \quad (3\text{-}10)$$

where *Patch_Az* and *Patch_Alt* are the patch azimuth and patch altitude respectively.

The office building was `xformed` into each sky patch rad file. A rad file was written for each of the 145 patches.

For example, part of patch 145:

```
# Patch145.rad
void light sky
0
0
3   233500  233500  233500

sky source 19623
0
0
4   0.00911   0.09541   0.99540   1

sky source 19624
0
0
4   0.02700   0.09196   0.99540   1

sky source 19625
0
0
4   0.04392   0.08519   0.99540   1

sky source 19626
0
0
4   0.05925   0.07534   0.99540   1

...continued...

sky source 19725
0
0
4   -0.02418   0.01002   0.99966   1

sky source 19726
0
0
4   -0.01002   0.02418   0.99966   1

sky source 19727
0
0
4   0.00873   0.00000   0.99996   1

sky source 19728
0
0
4   -0.00873   0.00000   0.99996   1

!xform  -e  -n  w1  office.rad
```

In the office.rad file, a rectangular ground plane made of `plastic` was placed on ground level to take into account the ground reflected component. This was of size 500m by 500m and reflectivity of 0.1. It was constructed using a 4-sided planar `polygon`, and was assumed to be matte and polished, thus the specularity and roughness were set to 0.

```
#added to office.rad

#ground
void   plastic       ground
0
0
5      0.1    0.1    0.1    0      0

ground polygon earth
0
0
12     -500   -500   0
        500   -500   0
        500    500   0
       -500    500   0
```

The `oconv` command was used to convert the rad files describing the patches and the office into octrees. For example, for patch 107:

```
% oconv for Patch107
oconv Patch107.rad > Patch107.oct
```

And as before for the office:

```
% oconv for office
oconv -f office.rad > RADoffice.oct
```

Radiance's `rtrace` program was next used to predict the illuminance due to a patch at every grid point. The ambient parameters were set to the ones determined to be most appropriate in section 3.1.4. For example, for patch 9:

```
%rtracesim for Patch 9

rtrace -w -h -I+ -ab 6 -aa 0.1 -ad 1024 -as 512 -ar 64 -dj .7 -ds .15 -dt .05 -dc .5 -dr 3 -dp
512 -sj .7 -st .15 -lr 8 -lw .002 Patch009.oct < grid.pts | rcalc -e
$1=($1*0.265+$2*0.670+$3*0.065)*179 > Patch009.out
```

Altogether, there were 145 executions of the `rtrace` program corresponding to the 145 patches. Each execution produced an output file that contained the predicted illuminances at every grid point.

3.2.3 Results

Equation 3-3 was used to calculate the actual illuminance at each grid point. To use this equation, however, first the daylight coefficients and the actual luminance of each of the 145 patches were to be determined.

The data produced by the `rtrace` program were inputted into the excel file Daylight_Coefficients.xls. These data were used to determine the daylight coefficients, *D*, since:

$$D = \left(\frac{E}{L_p \times S_p} \right) \tag{3-11}$$

where L_p and S_p are the luminance and the solid angle of the patch respectively.

Knowing the diameter of each small patch (=1°), it was possible to determine the solid angle of each small patch, S_{sp}:

$$S_{sp} = 2\pi \times \left(1 - \cos\left(\frac{1}{2} \right) \right) = 0.000239 str \tag{3-12}$$

And for the large patch:

$$S_p = \text{No. of } 1° \text{ patches} \times S_{sp} \tag{3-13}$$

Substituting for S_{sp}:

$$\rightarrow S_p = \text{No. of } 1° \text{ patches} \times 0.000239 \tag{3-14}$$

The central small patch was set to deliver 10,000 lux on an unobstructed horizontal surface. Hence, the luminance of the small patch used to determine the illuminances in *Radiance* was equal to:

$$L_{sp} = \frac{10{,}000}{S_{sp}} = \frac{10{,}000}{0.000239} = 41{,}798{,}253 cd/m^2 \tag{3-15}$$

In effect, the luminance of the small patch is the same as the luminance of the large patch. Thus, equation 3-11 converted to:

$$\rightarrow D = \left(\frac{E}{L_p \times S_p} \right) = \left(\frac{E}{41{,}798{,}253 \times S_p} \right) \tag{3-16}$$

Equation 3-16 was then used to determine the daylight coefficient for each patch at every grid point in the Daylight_Coefficients.xls file.

The actual luminance of each patch was determined using the global and diffuse illuminances monitored by a BRE station every five minutes during daylight hours for each month for a period of a year (1992). The Actual_L_p.xls excel file contains the actual luminance of each patch at the times when illuminance data were available. On some occasions the global and diffuse illuminance data provided by the BRE were negative, or there were no data available. In these cases, the spaces were filled up by the average of the patch luminances just before and just after the unspecified

luminance. The file is broken into months, and a macro was written to carry out the steps necessary to obtain the luminance of each patch at a five minute interval for every month.

Initially, the sun position in terms of the altitude, *Sun_Alt*, and the azimuth, *Sun_Az*, was determined (Figure 3.18).

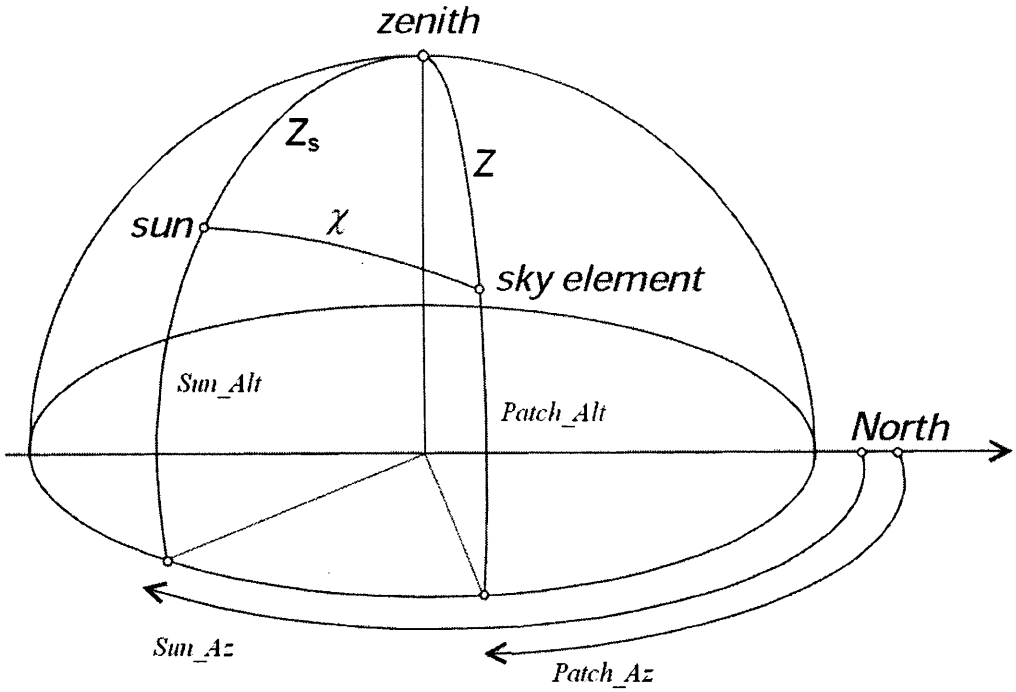

Figure 3.18: Angles defining the position of the sun and patch

The equation used to determine the azimuth angle uses true south as its reference. However, for the purpose of this paper, north is assumed to be the reference direction. As a consequence, certain checks and alterations had to be added in the code. The azimuth and altitude angles of the sun depend on the latitude (51.5° for London), day number, and most importantly, the time of the day, expressed as the number of days before solar noon[14]. The following two equations were used to compute the altitude and azimuth angles of the sun:

$$\sin(Sun\_Alt) = \cos(51.5)\cos(\delta)\cos(H) + \sin(51.5)\sin(\delta) \qquad (3\text{-}17)$$

$$\sin(Sun\_Az) = \frac{\cos(\delta)\sin(H)}{\cos(Sun\_Alt)} \qquad (3\text{-}18)$$

where δ and H are the solar declination and hour angle respectively. Both δ and H were determined, using the following equations:

$$\delta = 23.45 \sin\left[\frac{360}{364}(n-81)\right] \quad (3\text{-}19)$$

$$H = 15 \times (12 - ST) \quad (3\text{-}20)$$

where ST is the solar time and n is the day number starting with $n = 1$ for January 1st.

For most of solar work it is common to deal in solar time, where everything is measured relative to solar noon. There are two adjustments that must be made in order to connect local clock time to solar time. The first is a longitude adjustment that has to do with the way in which regions of the world are divided into time zones[14]. The longitude correction between local time and solar time is based on the time it takes for the sun to travel between the local time meridian and the observer's line of sight.

The second is a factor used to take into account the uneven way in which the earth moves around the sun[14]. As the earth moves through its orbit, the difference between a 24-hour day and a solar day changes following an expression known as the Equation of Time, EOT, measured in minutes:

$$EOT = 9.87 \sin(2b) - 7.53 \cos(b) - 1.5 \sin(B) \quad (3\text{-}21)$$

where

$$B = \frac{360}{364}(n-81) \quad (3\text{-}22)$$

As before, n is the day number.

The longitude correction and the Equation of Time were combined to give the final relationship between local standard time, CT, and solar time, ST:

$$ST = CT + 4\,(Local\ Time\ Meridian - Local\ Longitude)^{\circ} + \left(\frac{EOT}{60}\right) \quad (3\text{-}23)$$

For London, equation 3-23 reduces to:

$$\rightarrow ST = CT + \left(\frac{EOT}{60}\right) \quad (3\text{-}24)$$

Having determined the sun and patch altitude, the angular distance between the sun and the zenith, Z_s, and the patch and the zenith, Z, in degrees, was calculated. From Figure 3.18:

$$Z_s = 90 - Sun\_Alt \quad (3\text{-}25)$$

$$Z = 90 - Patch\_Alt \quad (3\text{-}26)$$

As mentioned earlier, the BRE station monitored the global and diffuse illuminances, $E_{glob,hor}$ and $E_{diff,hor}$, on an unobstructed horizontal surface. These figures

were used to determine the direct normal illuminance, $E_{dir,nor}$. Since:

$$E_{dir,hor} = E_{glob,hor} - E_{diff,hor} \tag{3-27}$$

Thus,

$$E_{dir,nor} = \frac{E_{dir,hor}}{\sin(Sun\_Alt)} \tag{3-28}$$

where $E_{dir,hor}$ is the direct illuminance on an unobstructed horizontal surface.

The sky model blend used was a composite of an overcast luminance pattern and a clear luminance pattern. The resultant patch luminance for a clear-overcast blend, $L_{co,p}$, was:

$$L_{co,p} = f_{cl}L_{cl,p} + f_{ov}L_{ov,p} \tag{3-29}$$

where $L_{cl,p}$ and $L_{ov,p}$ are the patch luminance of a clear and overcast sky respectively. Since $f_{ov} = 1 - f_{cl}$,

$$L_{co,p} = f_{cl}L_{cl,p} + (1 - f_{cl})L_{ov,p} \tag{3-30}$$

where f_{cl} is known as the weighting factor. The weighting factor depends on the clearness of the sky[9]. The more overcast a sky is, the smaller f_{cl} will be. Thus, for fully overcast skies, f_{cl} will be zero, while for progressively clearer skies, f_{cl} will tend to unity[11]. The factor f_{cl} is a function of the clearness index, ε, given by[15]:

$$\varepsilon = \frac{\left[\left(\frac{E_{diff,hor} + E_{dir,nor}}{E_{diff,hor}}\right) + 1.041Z_s^3\right]}{1 + 1.041Z_s^3} \tag{3-31}$$

where $E_{diff,hor}$, $E_{dir,nor}$, and Z_s are as specified earlier.

A simple linear mix based on the clearness index was used, where the fraction of the total due to the clear sky was:

$$f_{cl} = \begin{cases} \left(\frac{\varepsilon - \varepsilon_l}{\varepsilon_{ul} - \varepsilon_l}\right) & \varepsilon \le \varepsilon_{ul} \\ 1 & \varepsilon > \varepsilon_{ul} \end{cases} \tag{3-32}$$

The lower bound clearness index, ε_l, was set to 1, and the upper bound clearness index, ε_{ul}, was set to 1.1. Thus:

$$\rightarrow f_{cl} = \left(\frac{\varepsilon - 1}{0.1}\right) \quad \varepsilon \leq 1.1$$

$$1 \qquad \varepsilon \rangle \varepsilon_{ul} \tag{3-33}$$

To determine the patch luminance of a clear and an overcast sky, the ratio of the luminance of a patch to the zenith under a clear and overcast sky, $L_{cl,p}/L_{zcl}$ and $L_{ov,p}/L_{zcv}$, was determined according to BS ISO 15469:2004[3].

For a clear sky (according to Darula and Kittler (1967)):

$$\frac{L_{cl,p}}{L_{zcl}} = \frac{f(\chi)\phi(Z)}{f(Z_s)\phi(0)} \tag{3-34}$$

and for an overcast sky (according to Moon and Spencer (1942)):

$$\frac{L_{oc,p}}{L_{zoc}} = \frac{1 + 2\sin(Patch\_Az)}{3} \tag{3-35}$$

where $f(\chi)$ is the scattering indicatrix and $\phi(\chi)$ is the luminance gradation function.

The scattering indicatrix, $f(\chi)$, relates the relative luminance of a sky element to its angular distance from the sun:

$$f(\chi) = 1 + c\left[\exp(d\chi) - \exp\left(d\frac{\pi}{2}\right)\right] + e\cos^2(\chi) \tag{3-36}$$

and its value at the zenith is:

$$f(Z_s) = 1 + c\left[\exp(dZ_s) - \exp\left(d\frac{\pi}{2}\right)\right] + e\cos^2(Z_s) \tag{3-37}$$

where *c*, *d*, and *e* are known as the scattering indicatrix parameters and χ is the angular distance between the patch and the sun (Figure 3.18):

$$\chi = \cos^{-1}\left(\cos(Z_s)\cos(Z) + \sin(Z_s)\sin(Z)\cos\left(|Patch\_Az - Sun\_Az|\right)\right) \tag{3-38}$$

where Z_s, Z, *Patch_Az* and *Sun_Az* are as defined before.

The luminance gradation function, $\phi(Z)$, relates the luminance of a patch to its zenith angle:

$$\phi(Z) = 1 + a\exp\left(\frac{b}{\cos(Z)}\right) \qquad 0 \leq Z \langle \frac{\pi}{2}$$

$$\phi\left(\frac{\pi}{2}\right) = 1 \qquad \text{at the horizon} \tag{3-39}$$

where *a* and *b* are known as the luminance gradation parameters.

The parameters *a* to *e* in equations 3-36, 3-37 and 3-39, were selected from Table 3.7. This lists fifteen standard relative luminance distributions which are based on six groups of *a* and *b* values for the gradation function, and six groups of *c*, *d* and *e* values for the indicatrix function[3].

Type	Gradation group	Indicatrix group	*a*	*b*	*c*	*d*	*e*	Description of luminance distribution
1	I	1	4,0	-0,70	0	-1,0	0	**CIE Standard Overcast Sky,** Steep luminance gradation towards zenith, azimuthal uniformity
2	I	2	4,0	-0,70	2	-1,5	0,15	Overcast, with steep luminance gradation and slight brightening towards the sun
3	II	1	1,1	-0,8	0	-1,0	0	Overcast, moderately graded with azimuthal uniformity
4	II	2	1,1	-0,8	2	-1,5	0,15	Overcast, moderately graded and slight brightening towards the sun
5	III	1	0	-1,0	0	-1,0	0	**Sky of uniform luminance**
6	III	2	0	-1,0	2	-1,5	0,15	Partly cloudy sky, no gradation towards zenith, slight brightening towards the sun
7	III	3	0	-1,0	5	-2,5	0,30	Partly cloudy sky, no gradation towards zenith, brighter circumsolar region
8	III	4	0	-1,0	10	-3,0	0,45	Partly cloudy sky, no gradation towards zenith, distinct solar corona
9	IV	2	-1,0	-0,55	2	-1,5	0,15	Partly cloudy, with the obscured sun
10	IV	3	-1,0	-0,55	5	-2,5	0,30	Partly cloudy, with brighter circumsolar region
11	IV	4	-1,0	-0,55	10	-3,0	0,45	White-blue sky with distinct solar corona
12	V	4	-1,0	-0,32	10	-3,0	0,45	**CIE Standard Clear Sky, low luminance turbidity**
13	V	5	-1,0	-0,32	16	-3,0	0,30	**CIE Standard Clear Sky, polluted atmosphere**
14	VI	5	-1,0	-0,15	16	-3,0	0,30	Cloudless turbid sky with broad solar corona
15	VI	6	-1,0	-0,15	24	-2,8	0,15	White-blue turbid sky with broad solar corona

Table 3.7: Standard parameters

According to BS ISO 15469:2004, for a CIE standard clear sky in a polluted atmosphere, the standard parameters, *a*, *b*, *c*, *d*, and *e* are equal to -1, -0.32, 16, -3 and 0.30 respectively. Thus:

$$\rightarrow f(\chi)=1+16\left[\exp(-3\chi)-\exp\left(-3\times\frac{\pi}{2}\right)\right]+0.3\cos^2(\chi) \qquad (3\text{-}40)$$

$$\rightarrow f(Z_s)=1+16\left[\exp(-3Z_s)-\exp\left(-3\times\frac{\pi}{2}\right)\right]+0.3\cos^2(Z_s) \qquad (3\text{-}41)$$

and $$\rightarrow \phi(Z) = 1 + (-1)\exp\left(\frac{-0.32}{\cos(Z)}\right) \quad (3\text{-}42)$$

To determine the patch luminance of a clear and an overcast sky, the ratio of the luminance of a patch to the zenith under a clear and overcast sky was multiplied by a normalisation factor, *NF*.

Assuming a 1,000lx sky, for a clear sky:

$$NF_{cl} = \frac{1{,}000lx}{\sum_{1}^{p=145} E_{cl,p}} \quad (3\text{-}43)$$

where

$$E_{cl,p} = \frac{L_{cl,p}}{L_{zcl}} \times \cos(Z) \times SA_p \quad (3\text{-}44)$$

and for an overcast sky:

$$NF_{ov} = \frac{1{,}000lx}{\sum_{1}^{p=145} E_{oc,p}} \quad (3\text{-}45$$

where

$$E_{oc,p} = \frac{L_{oc,p}}{L_{zov}} \times \cos(Z) \times SA_p \quad (3\text{-}46)$$

Thus, the patch luminance for a clear sky:

$$L_{cl,p} = \frac{L_{cl,p}}{L_{zcl}} \times NF_{cl} \quad (3\text{-}47)$$

and for an overcast sky:

$$L_{ov,p} = \frac{L_{ov,p}}{L_{zov}} \times NF_{ov} \quad (3\text{-}48)$$

Having determined the clearness index earlier, and the patch luminance under a clear and overcast sky, it was then possible to use equation 3-30 to determine the patch luminance for a clear-overcast blend. The procedure was carried out for each patch where global and diffuse illuminance data were available by the BRE.

The total luminance of each patch for every month was then determined by adding the luminances of each patch within the month. To determine the actual luminance of a patch in an hour for a month, the sum was divided by twelve. For February, the summation was further multiplied by 28/29 as in 1992 there were 29

days in February instead of the usual 28. The final summation of each month was transferred into the Total sheet, where the results of each month were added up to determine the total luminance of each patch in a year.

Both daylight coefficients from the Daylight_Coefficients.xls file and total luminance of each patch from the Actual_Lp.xls file were transferred into the M_Results.xls file. There, equation 3-3 with n = 145 was used to determine the total klux-hours at every grid point for each month. The results were summed up to determine the annual klux-hours for every point (Figure 3.19, 3.20, 3.21 and 3.22 starting on the next page).

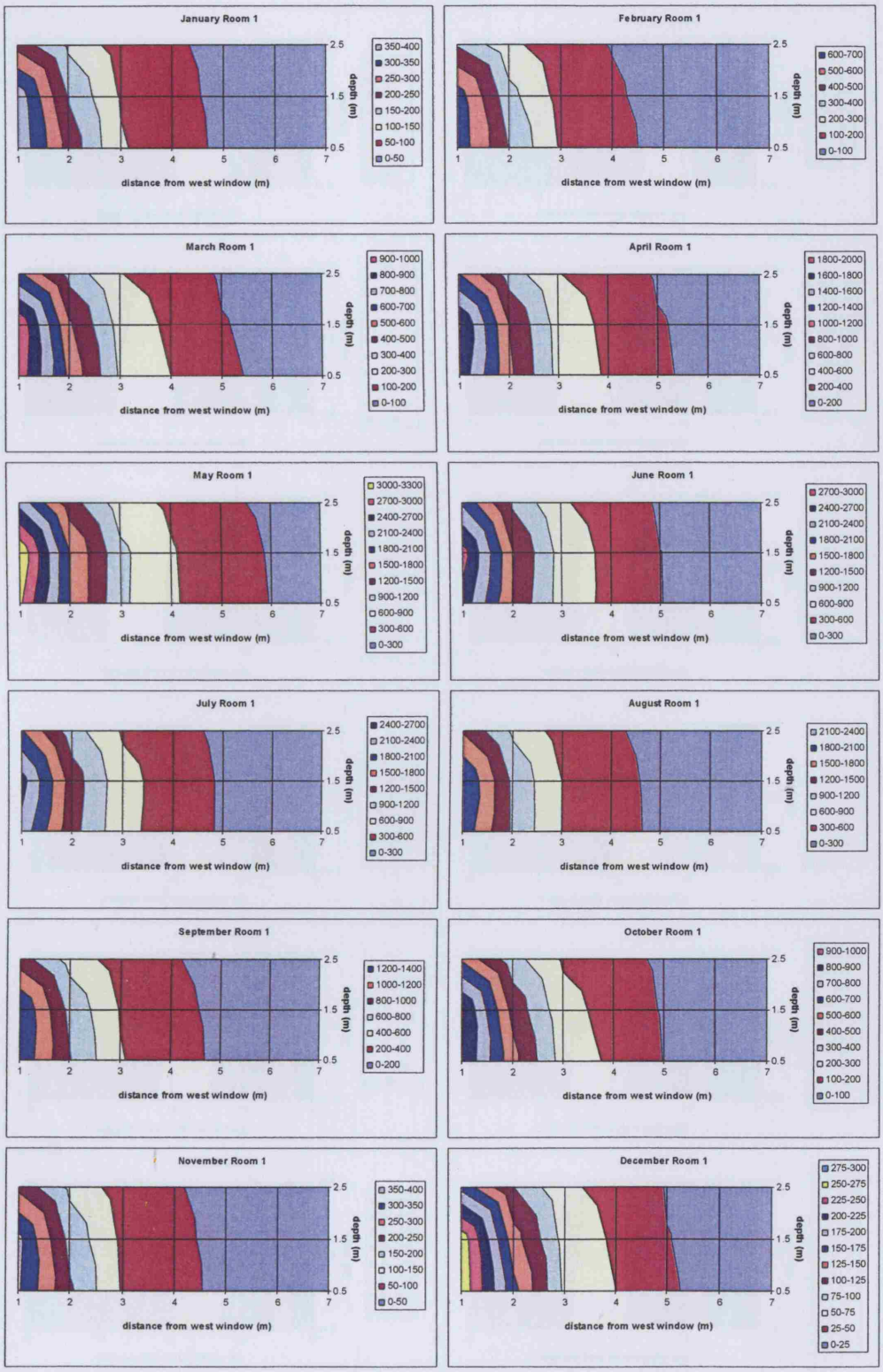

Figure 3.19: Total klux-hours for each month in Room 1

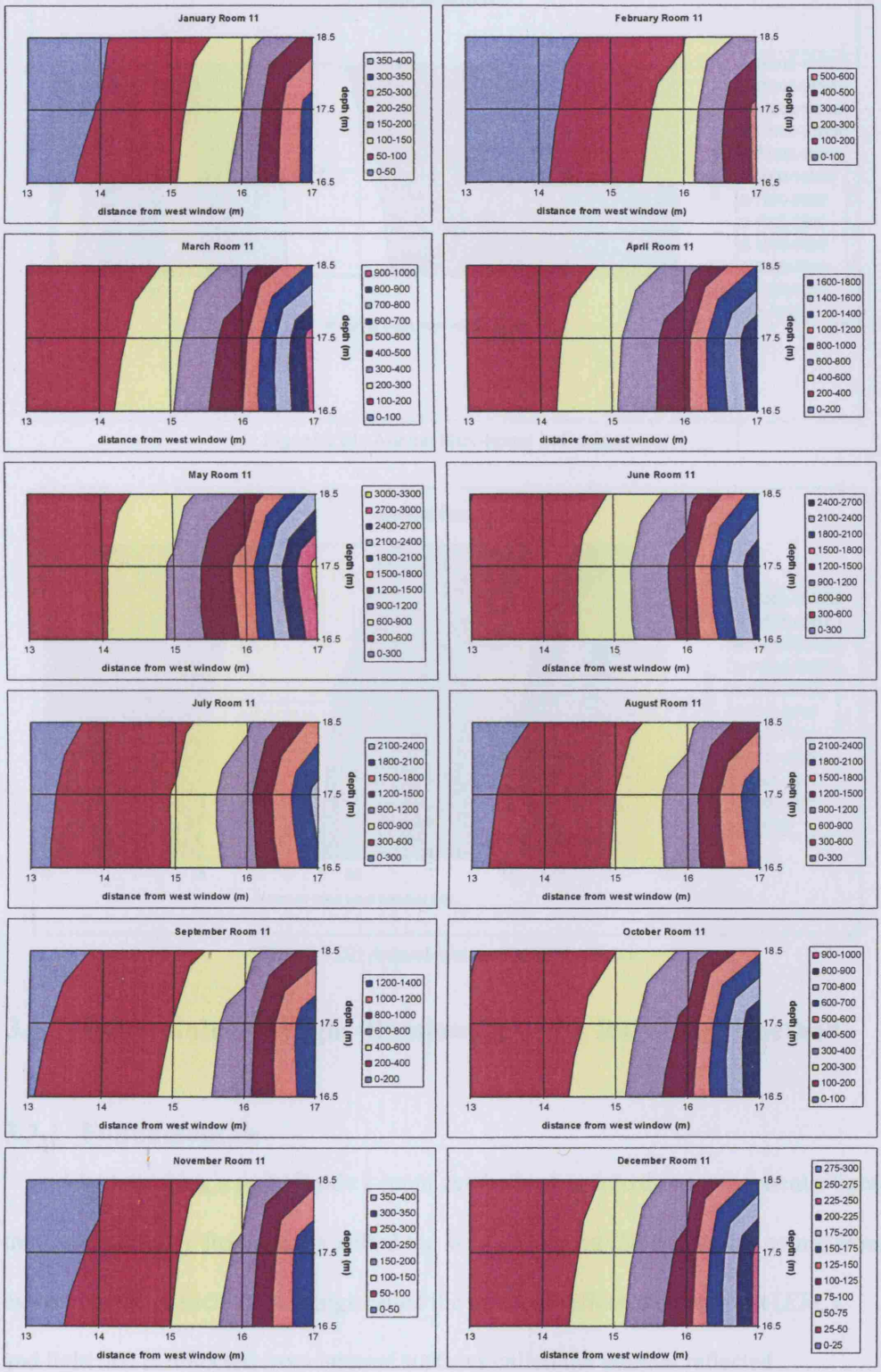

Figure 3.20: Total klux-hours for each month in Room 11

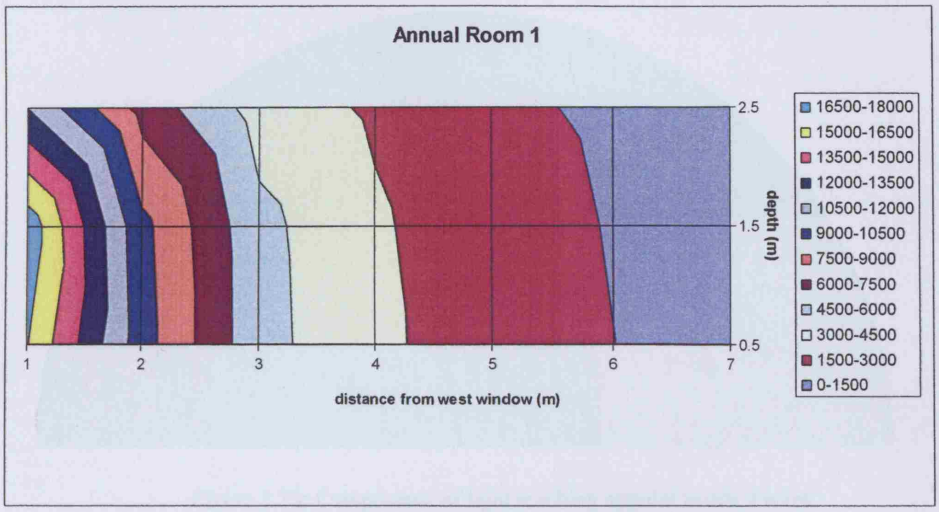

Figure 3.21: Annual klux-hours in Room 1

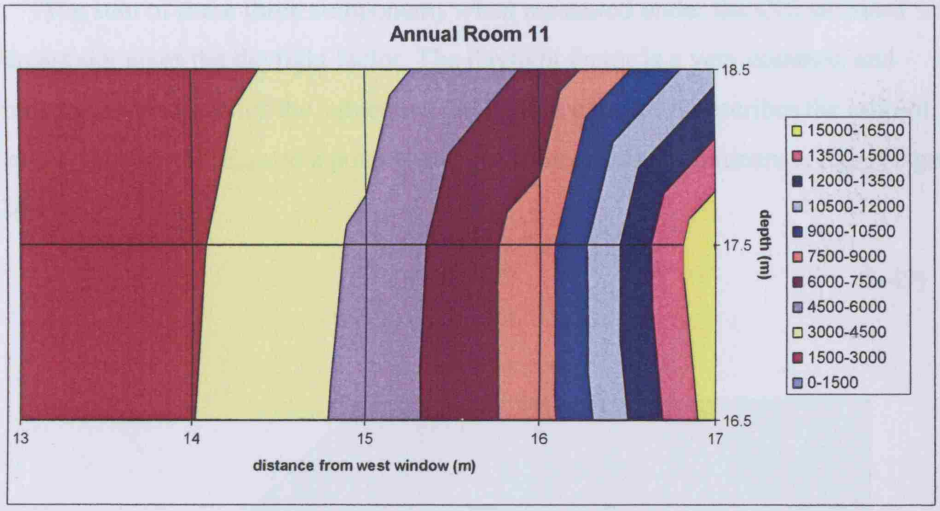

Figure 3.22: Annual klux-hours in Room 11

3.3 Determining daylight illuminance using Raynham's method

3.3.1 Fundamentals

Light reaching a point inside a room can be broken into three components: light that comes directly from the sky called the sky component (*SC*), light that comes from external surfaces such as buildings called the external reflected component (*ERC*), and light that is reflected from internal surfaces called the internal reflected component (*IRC*)[1](Figure 3.23):

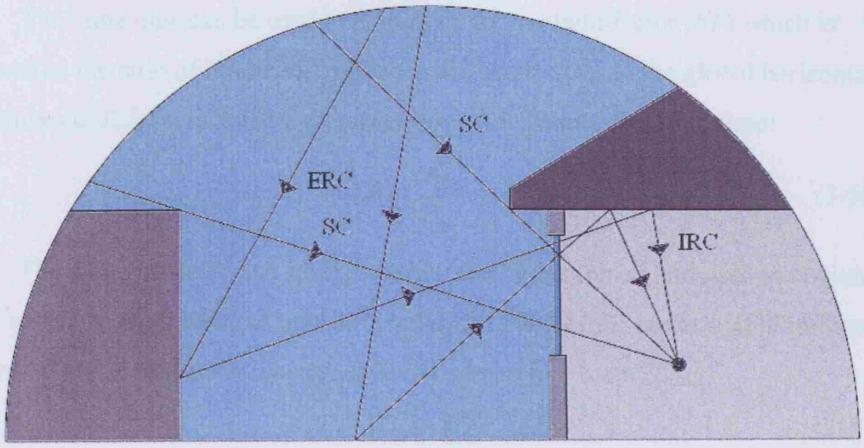

Figure 3.23: Components of light reaching appoint inside a room

The sum of these three components when measured under the CIE standard overcast sky gives the daylight factor. The daylight factor is a very common and simple to use measure for the subjective daylight in a room. It describes the ratio of internal illuminance, $E_{in,d}$, at a point to the global horizontal illuminance, $E_{out,d}$ (Figure 3.24):

$$DF = \frac{E_{in,d}}{E_{out,d}} \qquad (3\text{-}49)$$

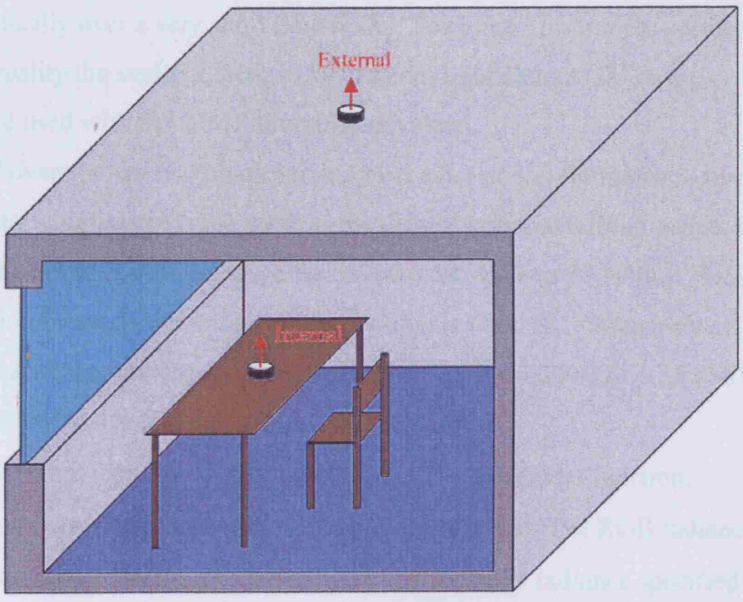

Figure 3.24: Defining the daylight factor

The same idea can be used to determine the sunlight factor (*SF*) which is defined as the ratio of internal illuminance at a point, $E_{in,s}$, to the global horizontal illuminance, $E_{out,s}$, due to the light direct from the sun at a specified time:

$$SF = \frac{E_{in,s}}{E_{out,s}} \tag{3-50}$$

The daylight factor and sunlight factor can be combined and used in conjunction with actual measured data of unobstructed diffuse and direct horizontal illuminance to determine the total illuminance produced at a point in a room, E_{total}:

$$E_{total} = (DF \times E_d) + (SF \times E_s) \tag{3-51}$$

where E_d and E_s are the measured unobstructed diffuse and direct horizontal illuminances.

3.3.2 Methodology

Radiance's sky generator program `gensky` was used to produce sun description and sky brightness distributions that correspond to the CIE overcast and clear skies. The overcast and clear CIE sky models used in *Radiance*, however, are representations of extreme sky types – densely overcast or completely clear. The brightness pattern of the sky can be quite difficult to characterise for all but heavily overcast conditions[4]. When clouds are present, the sky brightness distribution can change dramatically over a very short time scale. To convert from these perfect conditions to reality the sunlight factors (*SF*) and daylight factors (*DF*) were determined and used with the IDMP illuminance values.

The CIE overcast sky was characterised by the horizontal illuminance since the global horizontal illuminance is the same as the diffuse horizontal illuminance. It was assumed that the horizontal illuminance for an overcast sky was 10,000lux. *Radiance* uses a conversion factor for luminous efficacy which is fixed at 179lumens/watt [4]. Thus, the irradiance that corresponds to a 10,000lux sky is 10,000/179 = 55.866W/m^2. The altitude was set to 45° and the azimuth was set to 0°.

The output from the `gensky` program produced a brightness function, `skyfunc`, that was applied as a modifier to the `glow` material. The RGB radiance that the sky finally assumed was `skyfunc` multiplied by the RGB radiance specified for `glow`. For an overcast sky this was equal to unity for each channel. To minimise the errors that could occur because of the "infinite" horizon, an upside-down sky was

used to represent the luminous ground. The skyfunc modifier was applied to a 180-degree glow source of which the direction vector was pointing downwards. The ground reflectance was set to 0.1. This error reduction was also applied to all clear skies.

```
% ciesky.rad

# CIE overcast sky description (10,000 lux)with a 10% ground reflectance
!gensky -ang 45 0 -c -B 55.866

# this is the sky
skyfunc glow skyglow
0
0
4 1 1 1 0

skyglow source sky
0
0
4 0 0 1 180

skyfunc glow ground_glow
0
0
4 1 1 1 0


ground_glow source ground
0
0
4 0 0 -1 180

#this is the office octree being instanced into the sky
void instance building
7 RADoffice.oct -rz 0 -t 0 0 0
0
0
```

The oconv command was used to generate the octree from the rad file.

```
% oconv for ciesky
oconv ciesky.rad > ciesky.oct
```

The rtrace program was next used to predict the illuminance due to an overcast sky at every grid point. The ambient parameters were set to the ones determined to be most appropriate in section 3.1.4.

```
%rtracesim for the overcast sky

rtrace -w -h -I+ -ab 6 -aa 0.1 -ad 1024 -as 512 -ar 64 -dj .7 -ds .15 -dt .05 -dc .5 -dr 3 -dp
512 -sj .7 -st .15 -lr 8 -lw .002 ciesky.oct < grid.pts | rcalc -e
$1=($1*0.265+$2*0.670+$3*0.065)*179 > overcast.out
```

The rtrace program produced an output file that contained the predicted illuminances at every grid point under the CIE standard overcast sky.

In addition to the overcast sky analysis, a one day per month-hour clear sky analysis was carried out. For clear skies, in order to determine the direct contribution from the sun, both the global horizontal and the diffuse horizontal illuminance have to be determined. In order to do this, skies with and without the sun were modelled. The gensky program produced a scene description for the CIE standard sky distribution at a given month, day and time. The latitude was specified using the -a option, but since

the local time was used the -o option specifying the longitude was set to 0. The +s and -s options were used to reflect a sky with or without sun, respectively. For example, for a clear sky without sun (diffuse):

```
# SkyD022.rad (Clear sky without sun)

# March 15th at 10.00am. London, United Kingdom (latitude = 51.5°)

!gensky 3  15  10.00  -s -t 1.000000 -a 51.5 -o 0.000000 -m 0.000000

# this is the sky

skyfunc glow skyglow
0
0
4 1 1 1 0

skyglow source sky
0
0
4 0 0 1 180

skyfunc glow ground_glow
0
0
4 1 1 1 0

ground_glow source ground
0
0
4 0 0 -1 180

#this is the office octree being instanced into the sky

void instance building
7 RADoffice.oct -rz 0 -t 0 0 0
0
0
```

And for a clear sky with sun (global):

```
# SkyG022.rad (Clear sky with sun)

# November 15th at 11.00am. In London, United Kingdom (latitude = 51.5°)

 !gensky 11  15  11.00  +s -t 1.000000 -a 51.5 -o 0.000000 -m 0.000000

# this is the sky

skyfunc glow skyglow
0
0
4 1 1 1 0

skyglow source sky
0
0
4 0 0 1 180

skyfunc glow ground_glow
0
0
4 1 1 1 0

ground_glow source ground
0
0
4 0 0 -1 180

#this is the office octree being instanced into the sky

void instance building
7 RADoffice.oct -rz 0 -t 0 0 0
0
0
```

A sky was modelled for every hour where daylight was available on the 15th of each month. Thus, a total of 144 clear skies without sun and 144 clear skies with sun were simulated. When the rad files were finished, the information was compiled into octrees using the `oconv` command. For example, for a clear sky without sun (diffuse):

```
% oconv for SkyD010
oconv SkyD010.rad > SkyD010.oct
```

And for a clear sky with sun (global):

```
% oconv for SkyG127
oconv SkyG127.rad > SkyG127.oct
```

Radiance's `rtrace` program was next used to predict the illuminance due to a sky at every grid point. The ambient parameters were set to the ones determined to be most appropriate in section 3.1.4. For example, for a clear sky without sun (diffuse):

```
%rtracesim for SkyD032

rtrace -w -h -I+ -ab 6 -aa 0.1 -ad 1024 -as 512 -ar 64 -dj .7 -ds .15 -dt .05 -dc .5 -dr 3 -dp
512 -sj .7 -st .15 -lr 8 -lw .002 SkyD032.oct < grid.pts | rcalc -e
$1=($1*0.265+$2*0.670+$3*0.065)*179 > SkyD032.out
```

And for a clear sky with sun (global):

```
%rtracesim for SkyG080

rtrace -w -h -I+ -ab 6 -aa 0.1 -ad 1024 -as 512 -ar 64 -dj .7 -ds .15 -dt .05 -dc .5 -dr 3 -dp
512 -sj .7 -st .15 -lr 8 -lw .002 SkyDG080.oct < grid.pts | rcalc -e
$1=($1*0.265+$2*0.670+$3*0.065)*179 > SkyG080.out
```

Altogether, there were 288 executions of the `rtrace` program corresponding to each description of clear sky. Each execution produced an output file that contained the predicted illuminances at every grid point.

In order to determine the unobstructed horizontal illuminance, it was necessary to also simulate the same skies without instancing the office octree into the skies. For example, for a clear sky without sun (diffuse):

```
% SkyD22.rad (Clear sky without sun)
# March 15th at 10.00am. London, United Kingdom (latitude = 51.5°)
!gensky 3  15  10.00  -s -t 1.000000 -a 51.5 -o 0.000000 -m 0.000000
# this is the sky
skyfunc glow skyglow
0
0
4 1 1 1 0

skyglow source sky
0
0
4 0 0 1 180

skyfunc glow ground_glow
0
0
4 1 1 1 0

ground_glow source ground
0
0
4 0 0 -1 180
```

And for a clear sky with sun (global):

```
% SkyG22.rad (Clear sky with sun)

# November 15  at 11.00am. In London, United Kingdom (latitude = 51.5°)
 !gensky 11  15  11.00  +s -t 1.000000 -a 51.5 -o 0.000000 -m 0.000000

# this is the sky
skyfunc glow skyglow
0
0
4 1 1 1 0

skyglow source sky
0
0
4 0 0 1 180

skyfunc glow ground_glow
0
0
4 1 1 1 0

ground_glow source ground
0
0
4    0 0 -1 180
```

The octrees were compiled the same way as before using the `oconv` command. For example, for a clear sky without sun (diffuse):

```
% oconvSkyD42
oconv SkyD42.rad > SkyD42.oct
```

And for a clear sky with sun (global):

```
% oconvSkyG87
oconv SkyG87.rad > SkyG87.oct
```

For these, the text file grid.pts specified the XYZ location of only one measurement point and the XYZ vector direction of one photocell.

```
%grid.pts
#      x      y      z      x vector      y vector      z vector
       0      0      0          0             0             1
```

Next, the `rtrace` program was used the same way as when the office was instanced into the sky descriptions. For example, for a clear sky without sun (diffuse):

```
%rtracesim for SkyD132

rtrace -w -h -I+ -ab 6 -aa 0.1 -ad 1024 -as 512 -ar 64 -dj .7 -ds .15 -dt .05 -dc .5 -dr 3 -dp
512 -sj .7 -st .15 -lr 8 -lw .002 SkyD132.oct < grid.pts | rcalc -e
$1=($1*0.265+$2*0.670+$3*0.065)*179 > SkyD132.out
```

And for a clear sky with sun (global):

```
%rtracesim for SkyG11

rtrace -w -h -I+ -ab 6 -aa 0.1 -ad 1024 -as 512 -ar 64 -dj .7 -ds .15 -dt .05 -dc .5 -dr 3 -dp
512 -sj .7 -st .15 -lr 8 -lw .002 SkyDG11.oct < grid.pts | rcalc -e
$1=($1*0.265+$2*0.670+$3*0.065)*179 > SkyG11.out
```

Altogether, there were 288 executions of the `rtrace` program corresponding to each description of clear sky. Each execution produced an output file that contained the predicted illuminances at every grid point.

3.3.3 Results

Data manipulation took place in the excel file R_Results.xls. The daylight factors were determined using the illuminances produced by the `rtrace` program for the CIE standard overcast sky. Using equation 3-47 with $E_{out,d}$ = 10,000lux:

$$\rightarrow DF = \frac{E_{in,d}}{10{,}000} \qquad (3\text{-}52)$$

The daylight factors were the same for all months.

The diffuse and global unobstructed external horizontal illuminance data, $E_{out,d}$ and $E_{out,g}$, for each sky were used to determine the direct unobstructed illuminance, $E_{,out,s}$:

$$E_{out,s} = E_{out,g} - E_{out,d} \qquad (3\text{-}53)$$

In the same way, the direct illuminance, $E_{in,s}$, inside the office was determined using the internal diffuse and global illuminances, $E_{in,d}$ and $E_{in,g}$, produced by the `rtrace` program:

$$E_{in,s} = E_{in,g} - E_{in,d} \qquad (3\text{-}54)$$

Sometimes, the global and diffuse illuminances were very close to one another, resulting in negative values. In this case the direct internal illuminance was set to zero.

Having determined the direct unobstructed external illuminance and the internal direct illuminance, it was possible to determine the sunlight factor using equation 3-50.

Actual measured data of unobstructed diffuse and direct horizontal illuminance were provided by the BRE. These were monitored in a station every five minutes during daylight hours for each month for a period of a year (1992). For each hour an average was determined for the global and diffuse horizontal illuminances which, were used to calculate the average direct external horizontal illuminance, $E_{avgext,s}$:

$$E_{avgext,s} = E_{avgext,g} - E_{avgext,d} \qquad (3\text{-}55)$$

For example, for January 1992:

Hour	**9**	**10**	**11**	**12**	**13**	**14**	**15**	**16**
Start	8:31 AM	9:31 AM	10:31 AM	11:31 AM	12:31 PM	1:31 PM	2:31 PM	3:31 PM
End	9:30 AM	10:30 AM	11:30 AM	12:30 PM	1:30 PM	2:30 PM	3:30 PM	4:30 PM
$E_{avgext,g}$ (lux)	3520.43	9206.17	14497.76	16297.30	14954.20	11483.58	6232.38	1723.53
$E_{avgext,d}$ (lux)	3237.95	7622.84	10967.21	11946.86	11223.73	9076	5226.13	1555.75
$E_{avgext,s}$ (lux)	282.48	1583.34	3530.55	4350.44	3730.47	2407.58	1006.25	167.79

The average diffuse horizontal illuminance was used in conjunction with the daylight factor to determine the actual diffuse illuminance. Using equation 3-49, the actual diffuse illuminance, $E_{d,\,ave}$, is equal to:

$$\rightarrow E_{avg,d} = DF \times E_{avgext,d} \tag{3-56}$$

The average direct horizontal illuminance, on the other hand, was used in conjunction with the sunlight factor to determine the actual direct illuminance. Using equation 3-50, the actual direct illuminance, $E_{avg,s}$, is equal to:

$$\rightarrow E_{avg,s} = SF \times E_{avgext,s} \tag{3-57}$$

Knowing the actual direct and diffuse illuminance values, it was possible to determine the actual average global illuminance, $E_{avg,g}$:

$$\rightarrow E_{avg,g} = E_{avg,s} + E_{avg,d} \tag{3-58}$$

The total klux-hours per month, E_{total}, at each measuring point is then equal to:

$$E_{total} = \frac{E_{avg.g} \times number\_of\_days\_in\_month}{1000} \tag{3-59}$$

For example for January at 13:00 and XYZ co-ordinates of 3, 8.9, 0.7, $E_{Jan,total}$ is equal to:

$$\rightarrow E_{Jan,total} = \frac{321.231 \times 31}{1000} = 9.958 klux - hrs$$

The total klux-hours at every grid point were determined for each month following the above process. The results were summed up to determine the annual klux-hours for every point (Figures 3.25, 3.26, 3.27 and 3.28 starting on the next page).

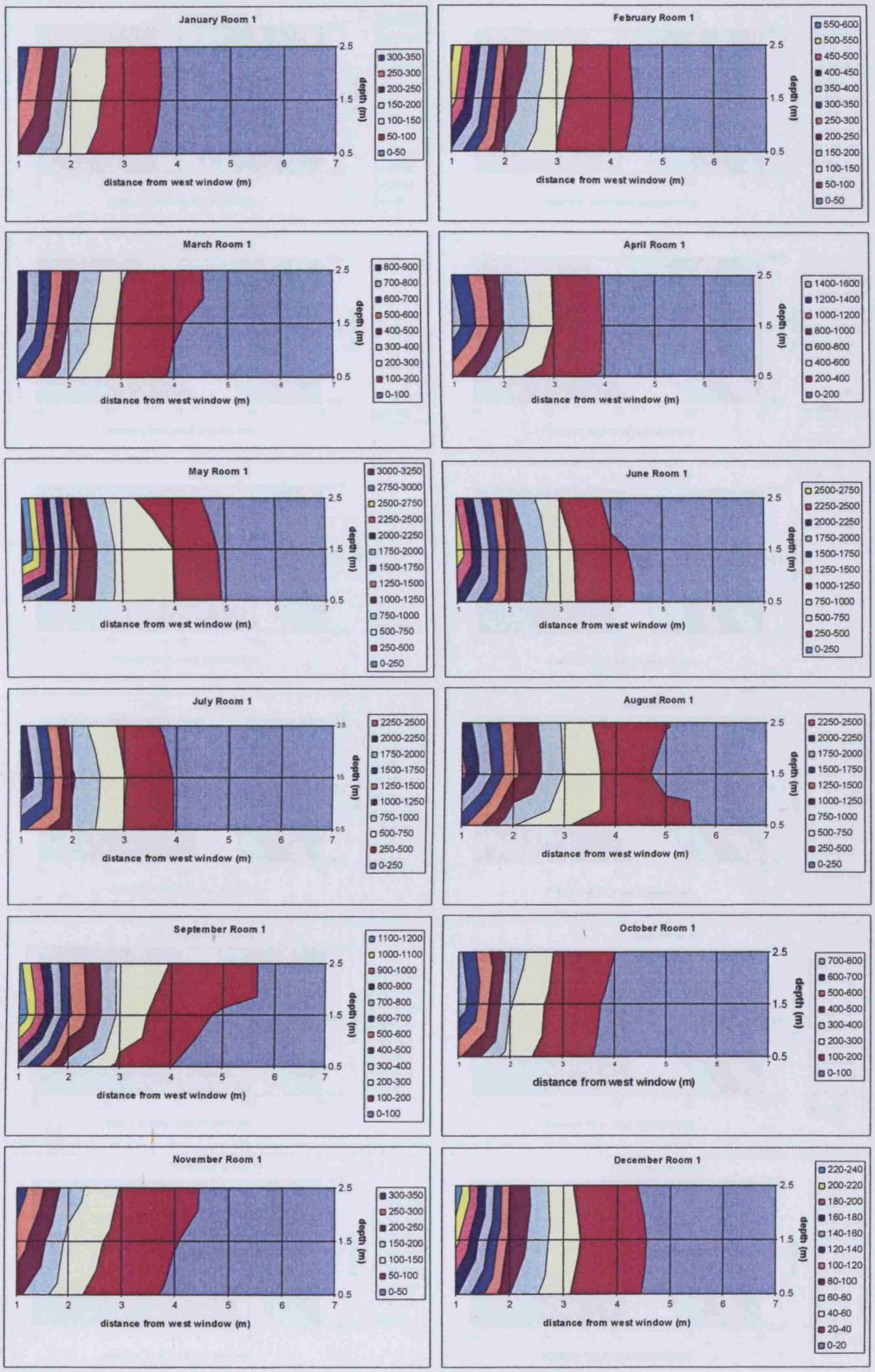

Figure 3.25: Total klux-hours for each month in Room 1

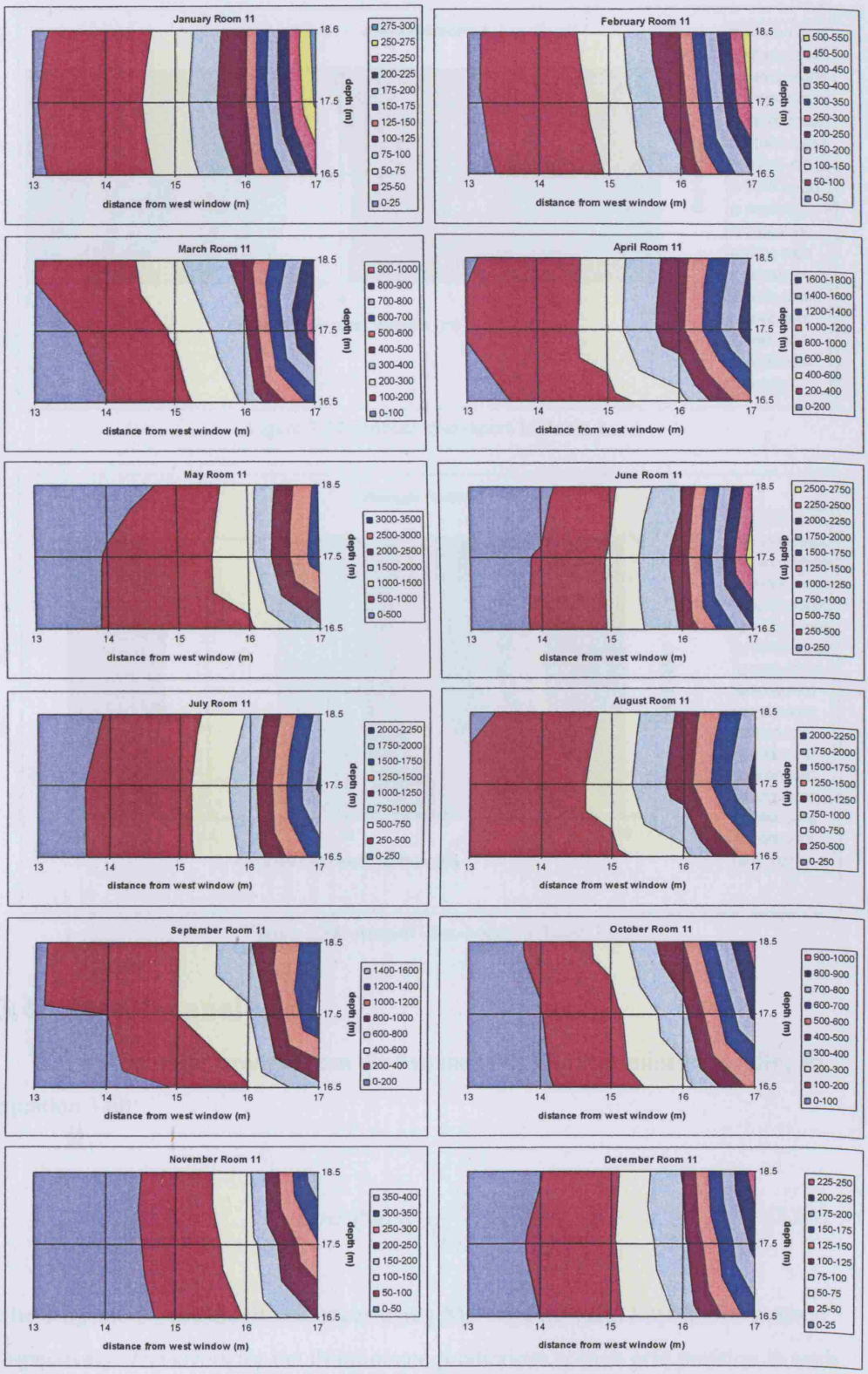

Figure 3.26: Total klux-hours for each month in Room 11

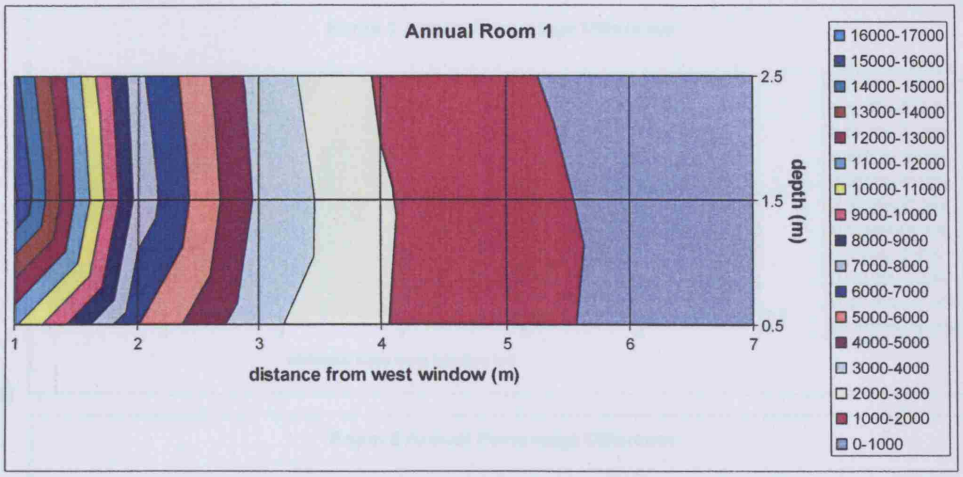

Figure 3.27: Annual klux-hours in Room 1

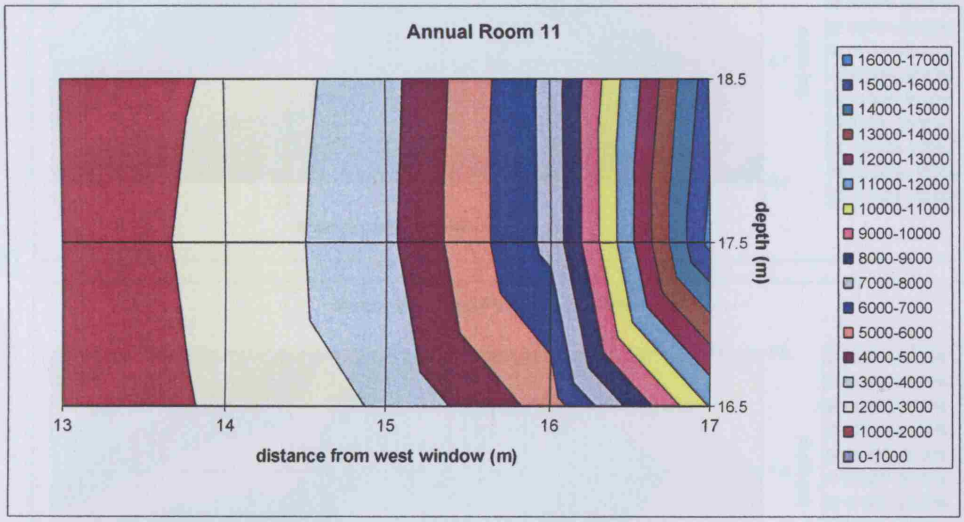

Figure 3.28: Annual klux-hours in Room 11

3.4 Results analysis

The percentage error between the two methods was determined according to equation 3.60:

$$Error(\%) = \frac{E_M - E_R}{\left((E_M + E_R)/2\right)} \tag{3.60}$$

where E_R and E_M are the illuminances using Mardaljevic's and Raynham's method respectively. The errors for the illuminance predictions at each grid position in each room are shown in Figure 3.29.

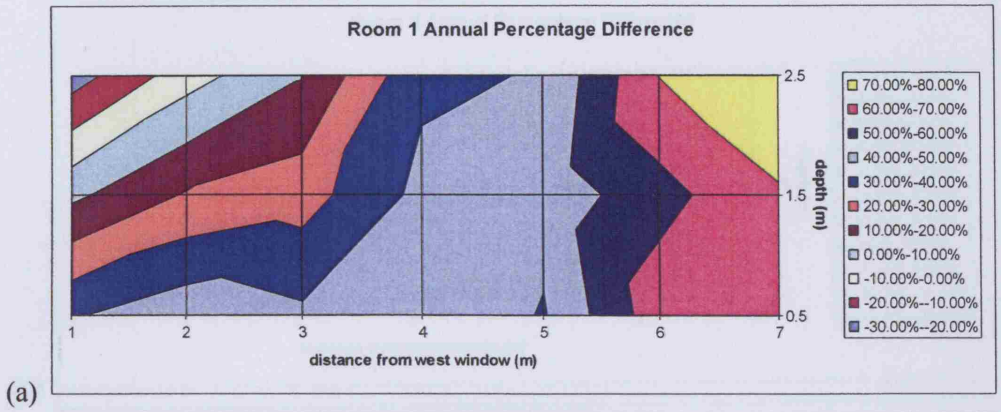

(a)

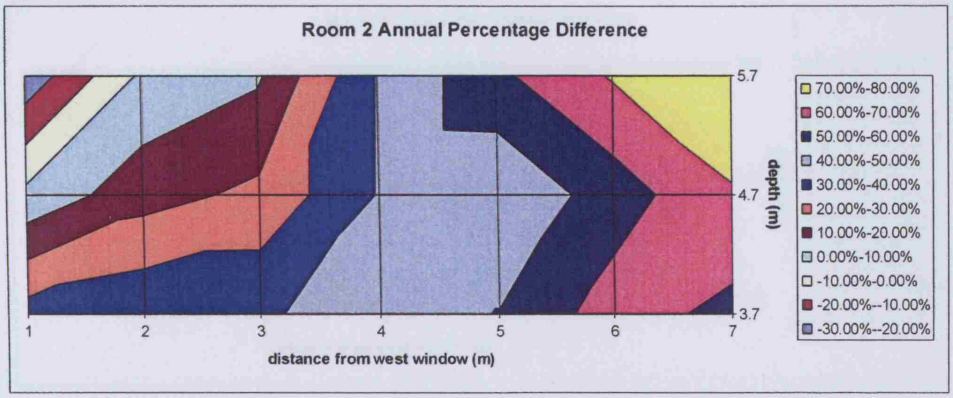

(b)

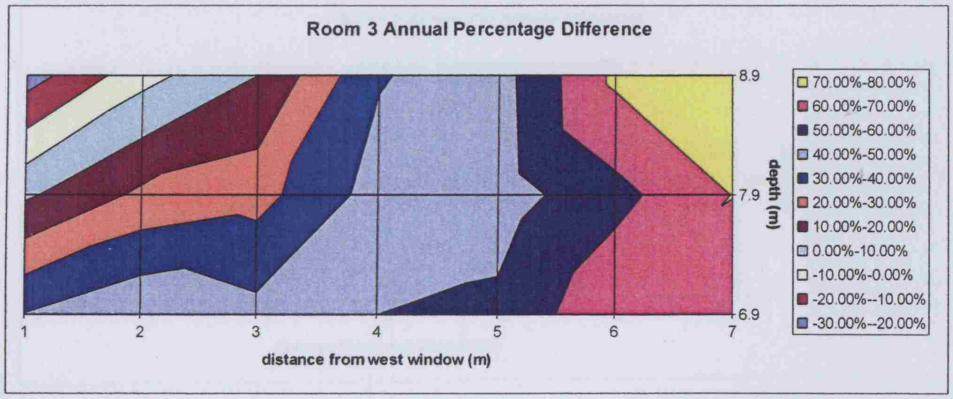

(c)

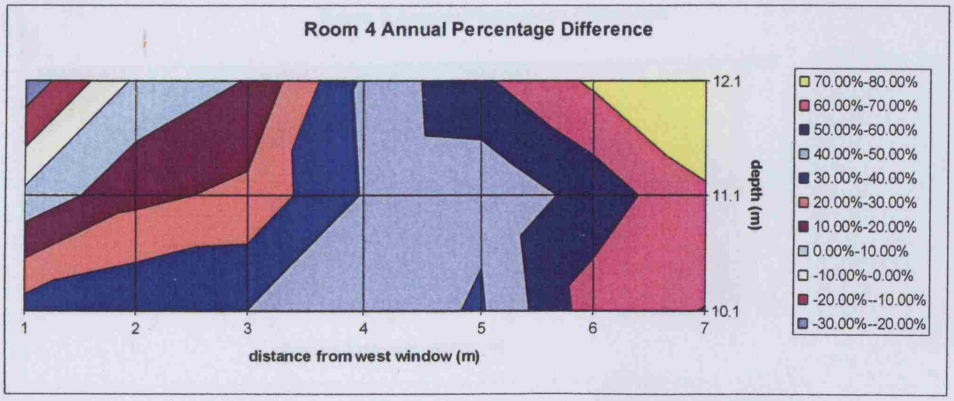

(d)

Figure 3.29 (a), (b), (c), (d): Room 1 to 4 annual percentage difference

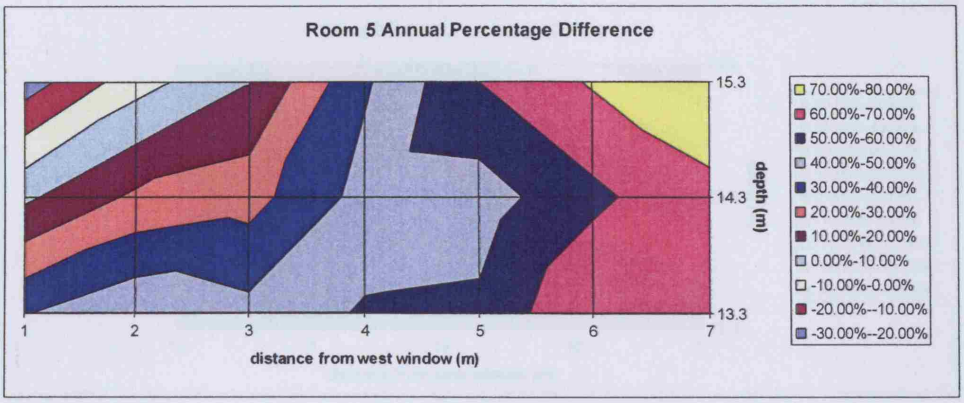

(e)

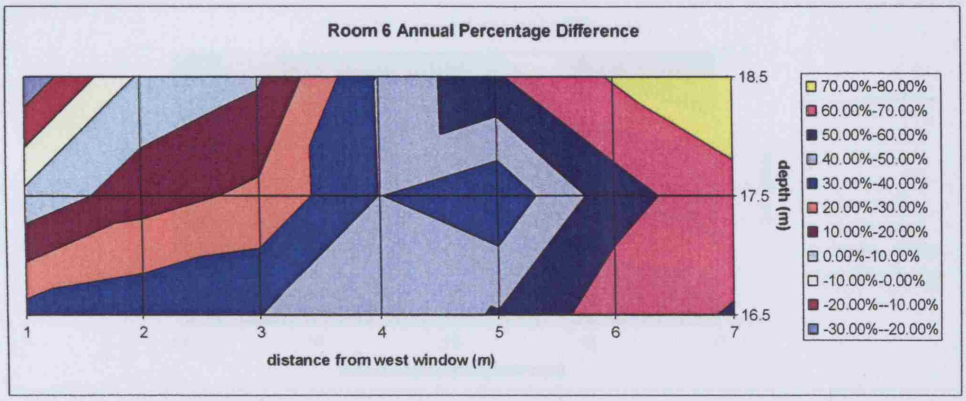

(f)

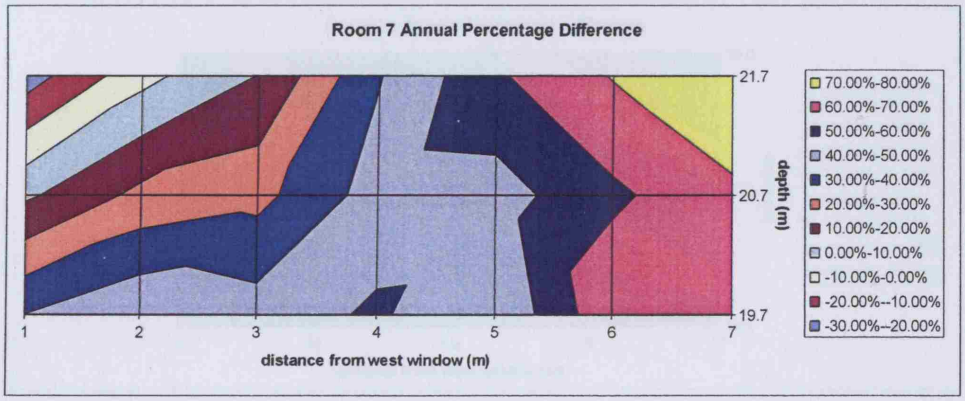

(g)

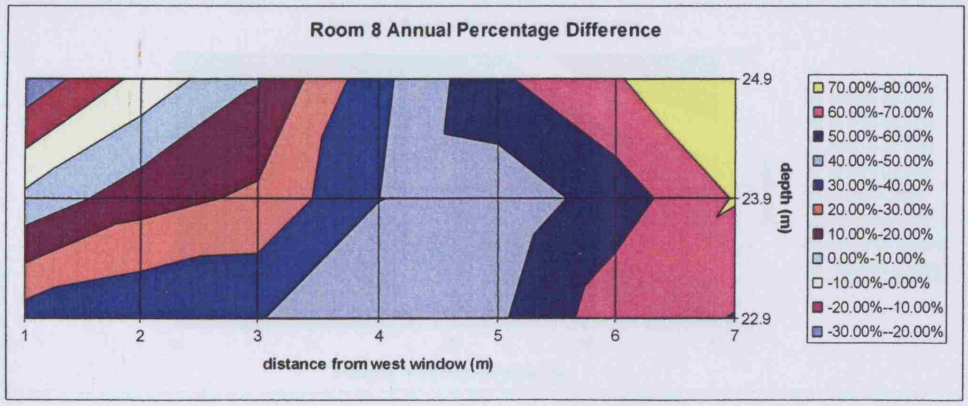

(h)

Figure 3.29 (e), (f), (g), (h): Room 5 to 8 annual percentage difference

(i)

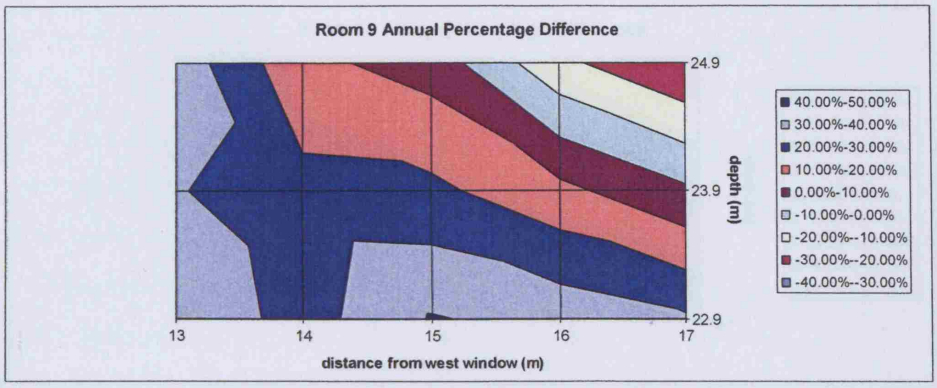

(j)

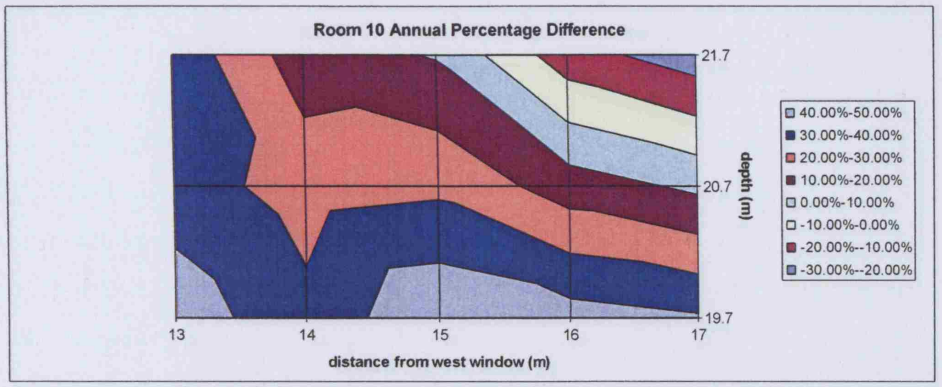

(k)

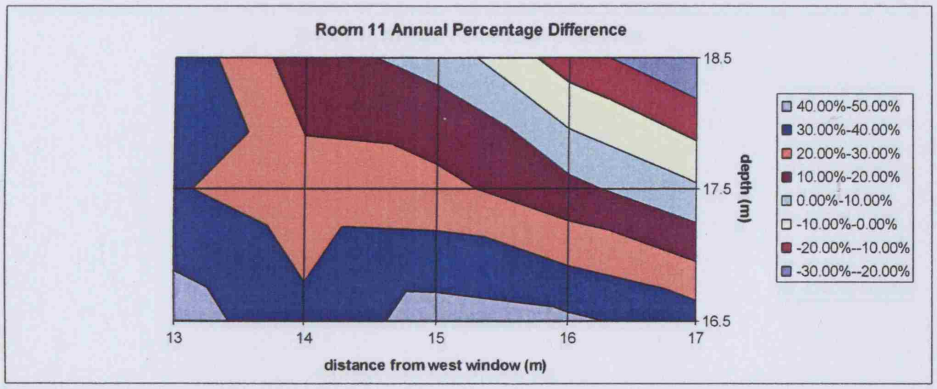

(l)

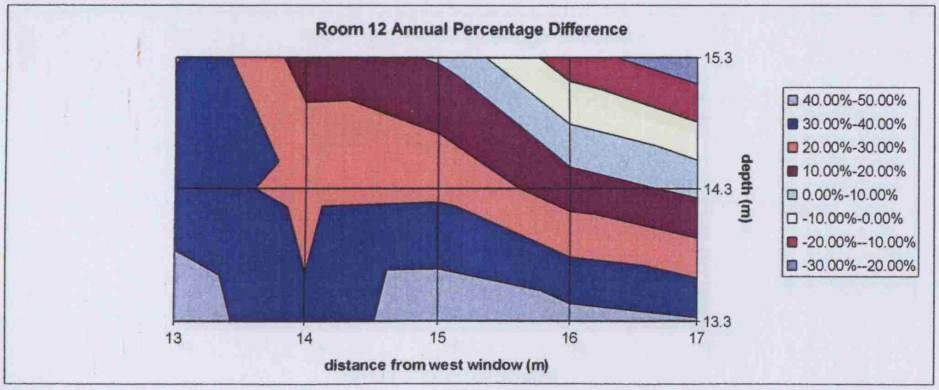

Figure 3.29 (i), (j), (k), (l): Room 9 to 12 annual percentage difference

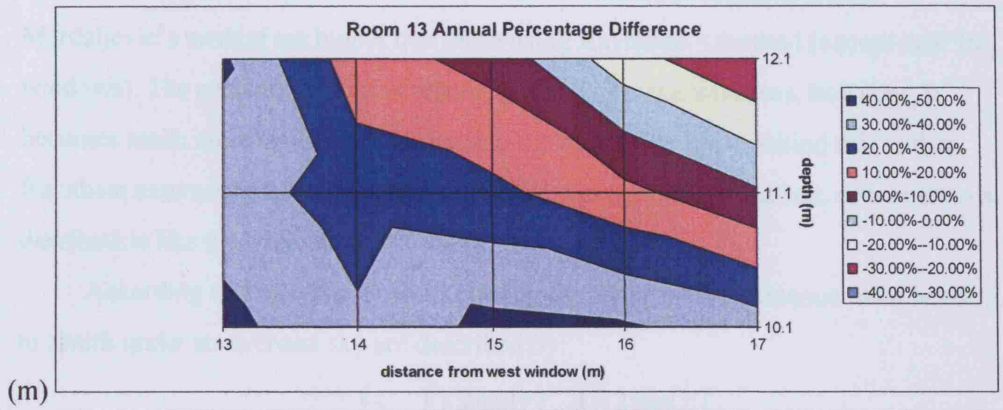

(m)

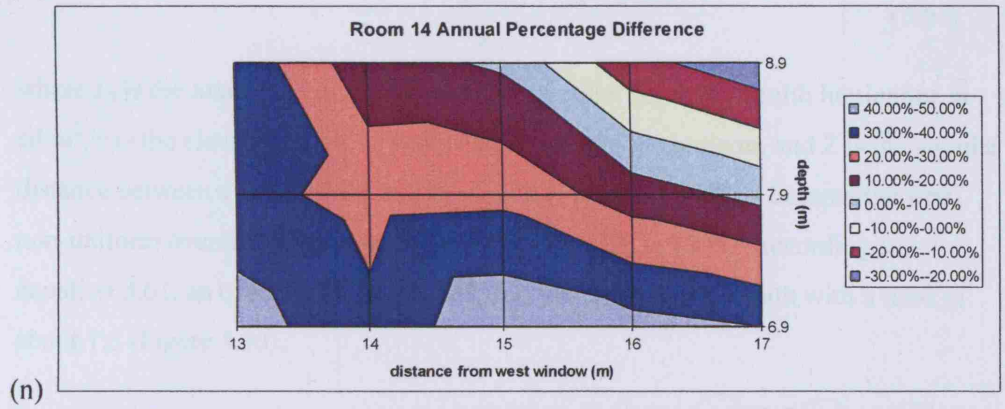

(n)

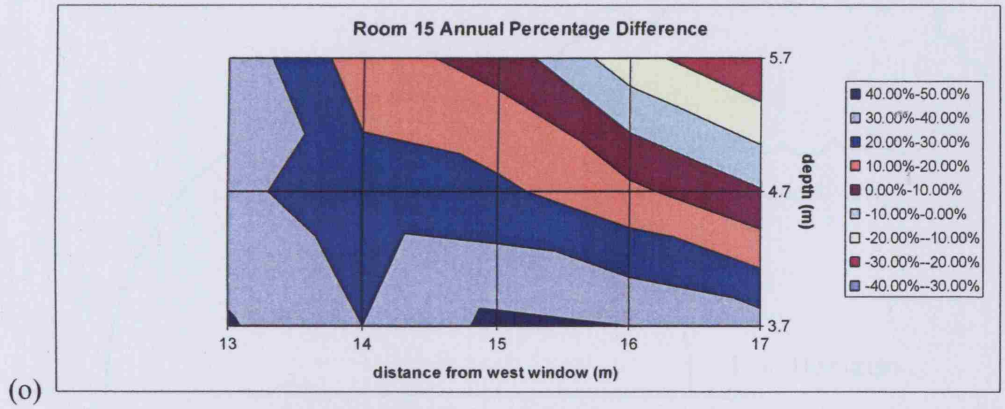

(o)

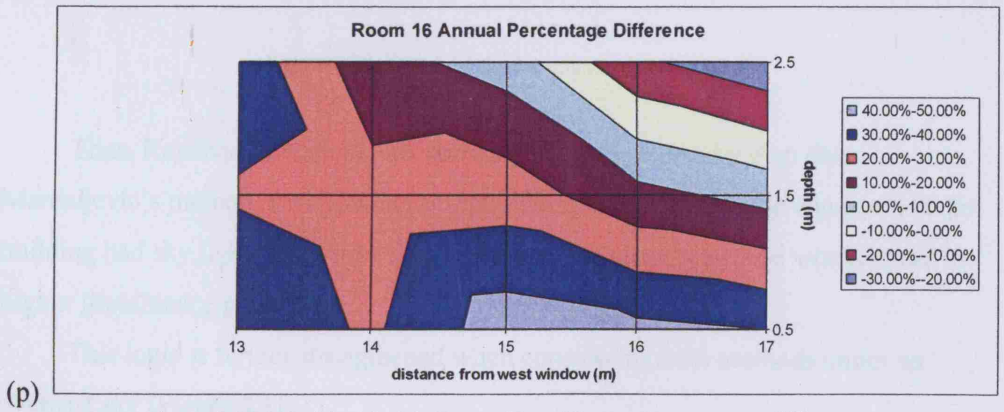

(p)

Figure 3.29 (m), (n), (o), (p): Room 13 to 16 annual percentage difference

From Figure 3.29, it is obvious that the illuminance predictions using Mardaljevic's method are higher that those using Raynham's method (except near the windows). The percentage error is relatively small near the windows, however, it becomes much more significant deeper into the room. The logic behind this is that Raynham assumes that all the light from the sky, as opposed to the sun, comes from a distribution like the overcast sky.

According to Moon and Spenser (1942), the changes of luminance from horizon to zenith under an overcast sky are described by:

$$\frac{L_\gamma}{L_Z} = \frac{1+2\sin(\gamma)}{3} = \frac{1+2\cos(Z)}{3} \qquad (3.61)$$

where L_γ is the luminance of the sky element in cd/m^2, L_Z is the zenith luminance in cd/m^2, γ is the elevation angle of a sky element above the horizon, and Z is the angular distance between a sky element and the zenith (Figure 3.18). This became the first non-uniform overcast sky standard adapted by the CIE in 1955. According to equation 3.61, an overcast sky has a dark horizon and brighter zenith with a ratio of about 1:3 (Figure 3.30).

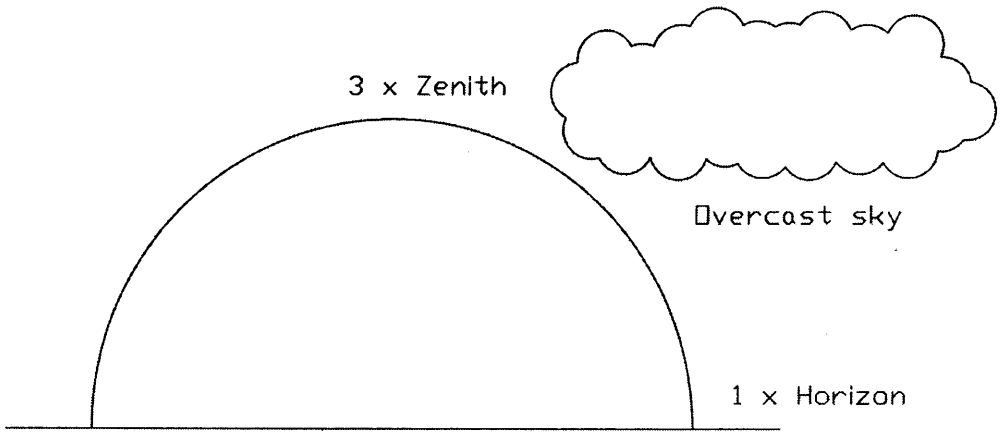

Figure 3.30: Overcast sky luminance distribution

Thus, Raynham's method puts more light higher in the sky than does Mardaljevic's method, thus yielding to lower illuminances from side windows. If the building had sky lights it would be expected that Raynham's method would result in higher illuminance predictions.

This logic is further strengthened when considering both methods under an overcast sky (Figure 3.31).

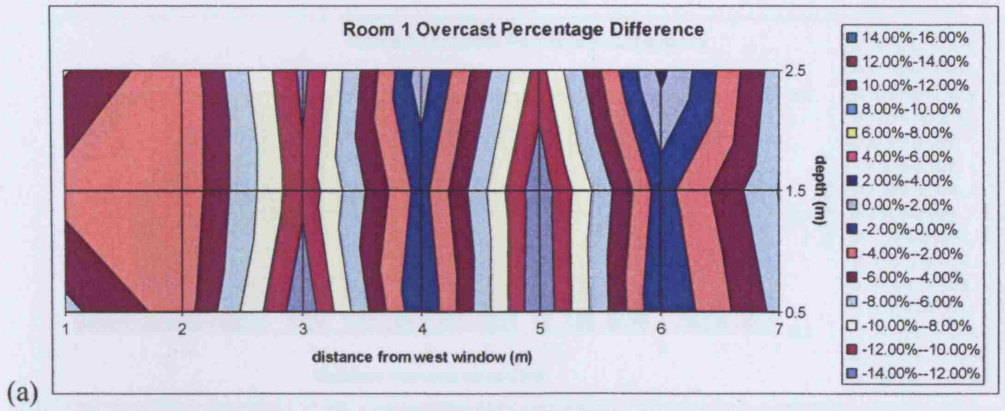

(a)

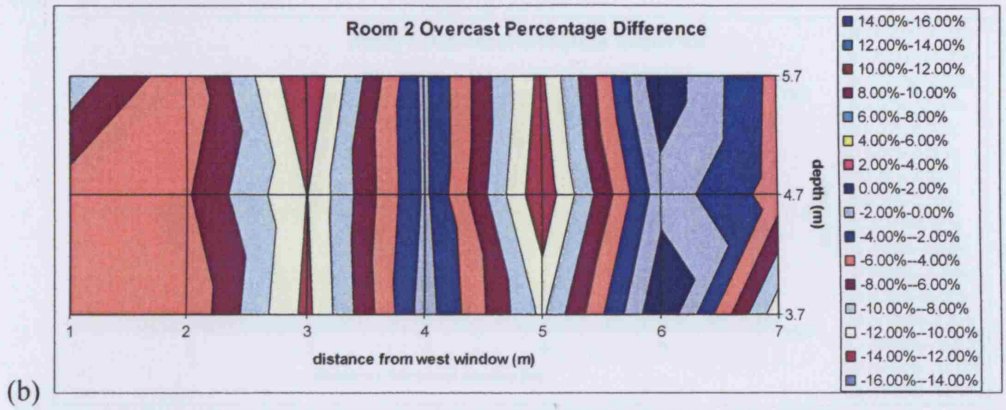

(b)

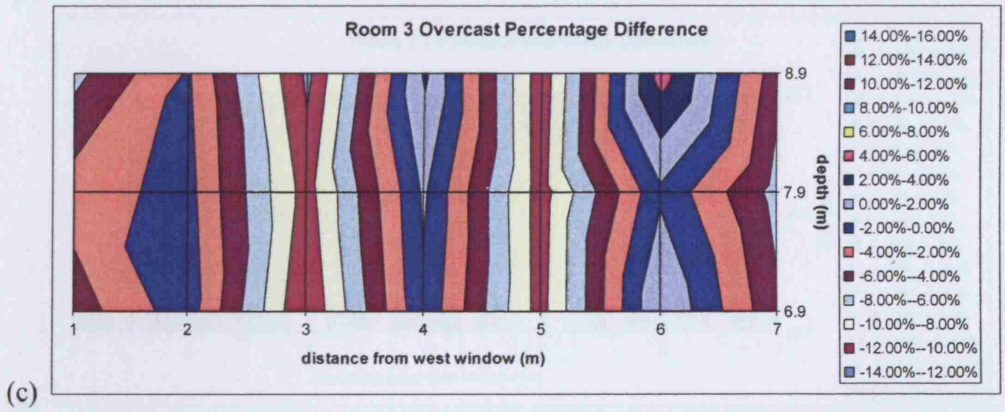

(c)

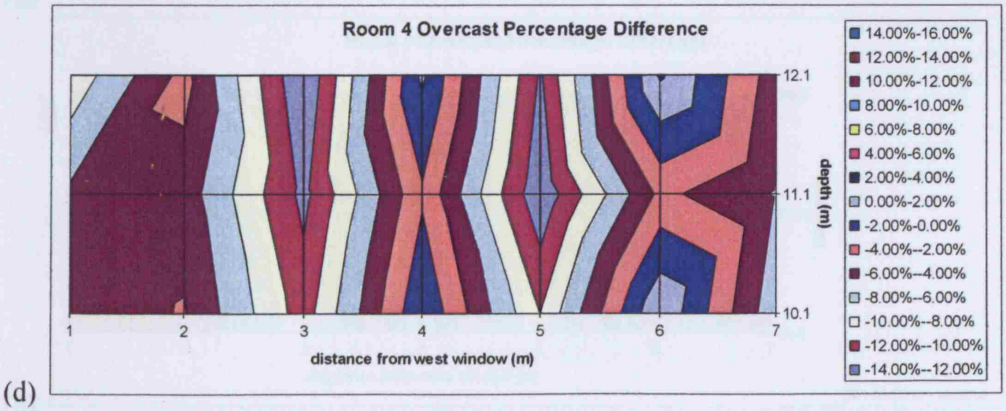

(d)

Figure 3.31 (a), (b), (c), (d): Room 1 to 4 overcast percentage difference

(e)

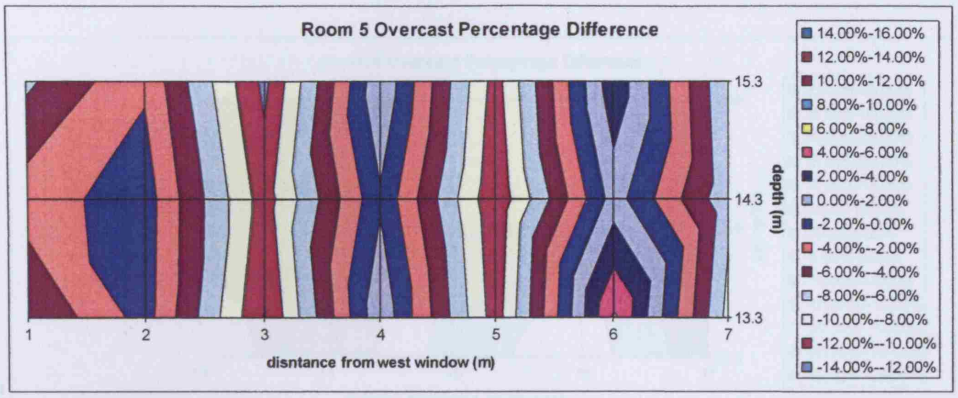

(f)

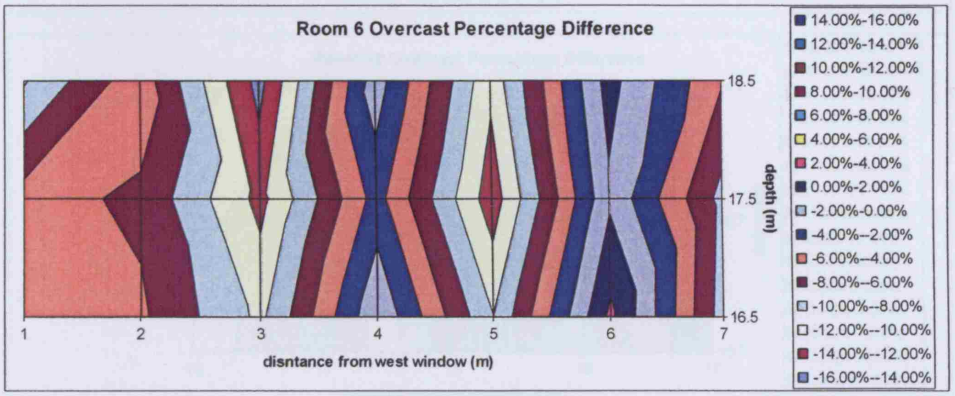

(g)

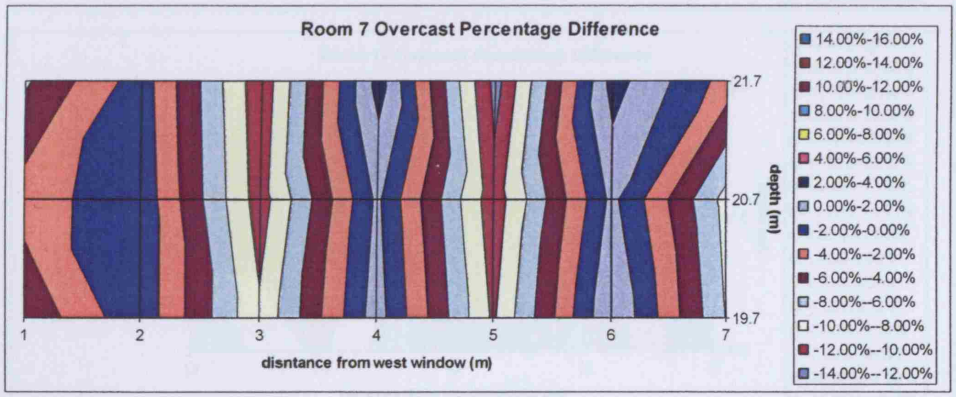

(h)

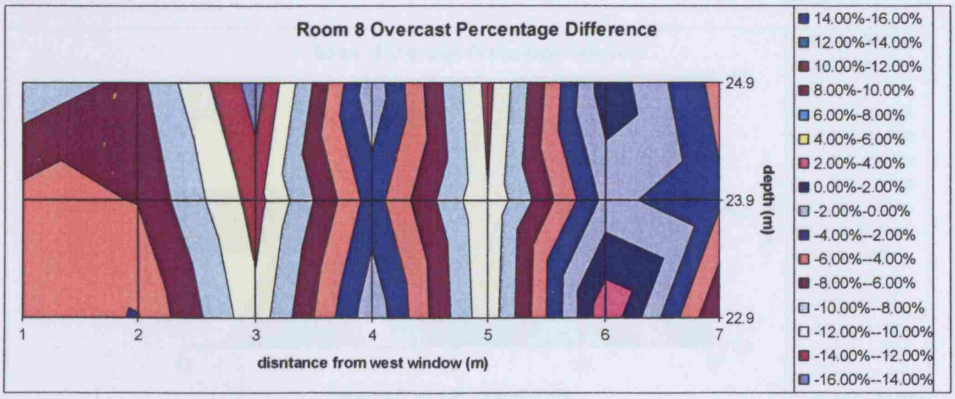

Figure 3.31 (e), (f), (g), (h): Room 5 to 8 overcast percentage difference

(i)

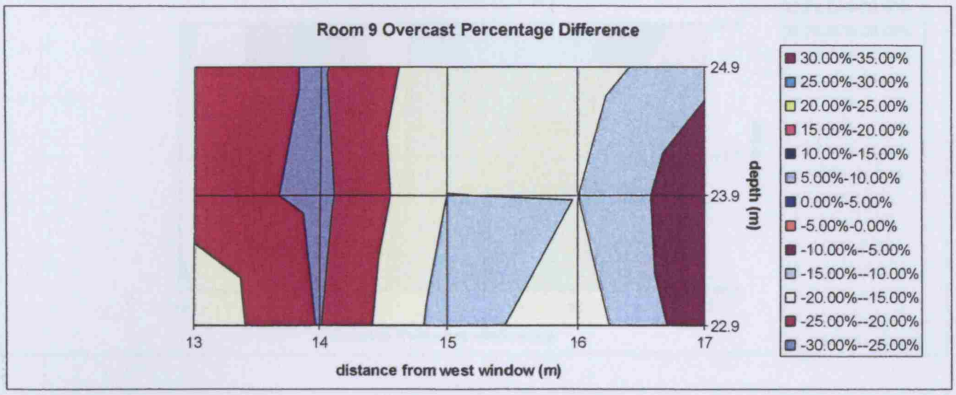

(j)

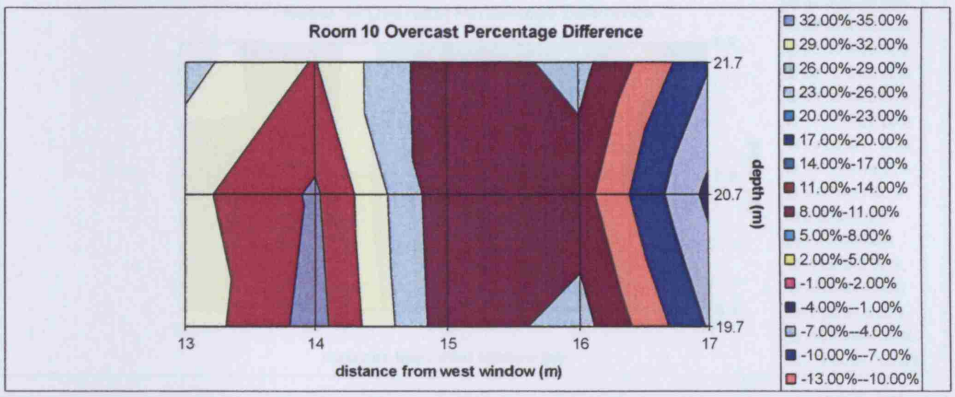

(k)

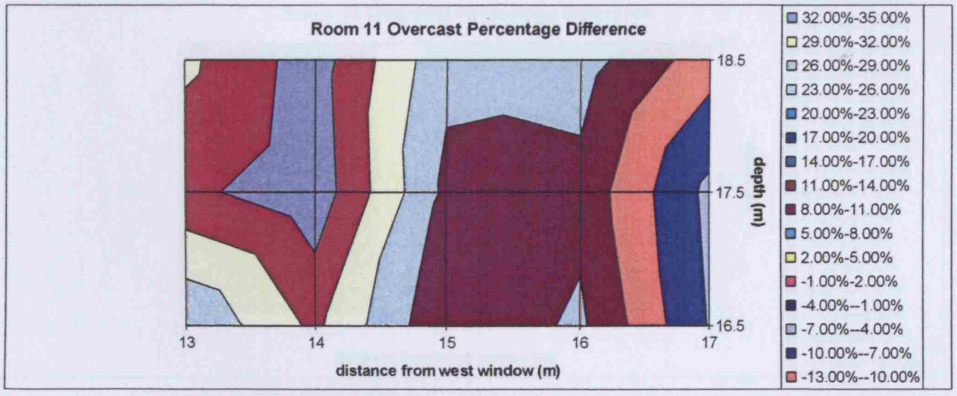

(l)

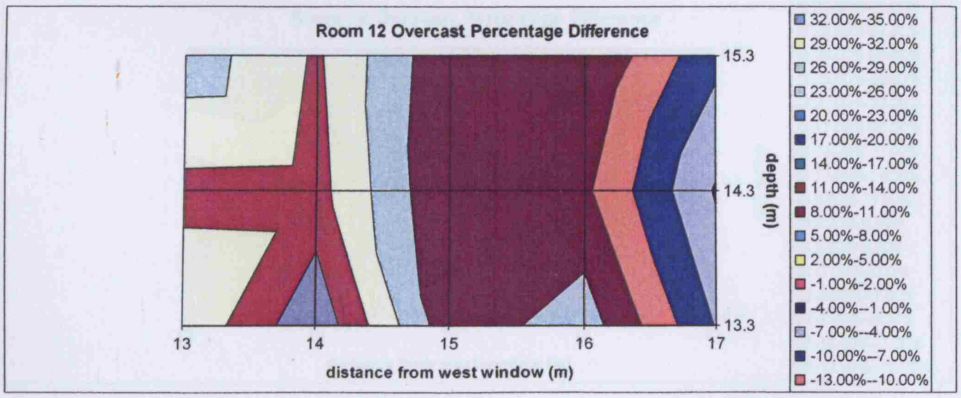

Figure 3.31 (i), (j), (k), (l): Room 9 to 12 overcast percentage difference

(m)

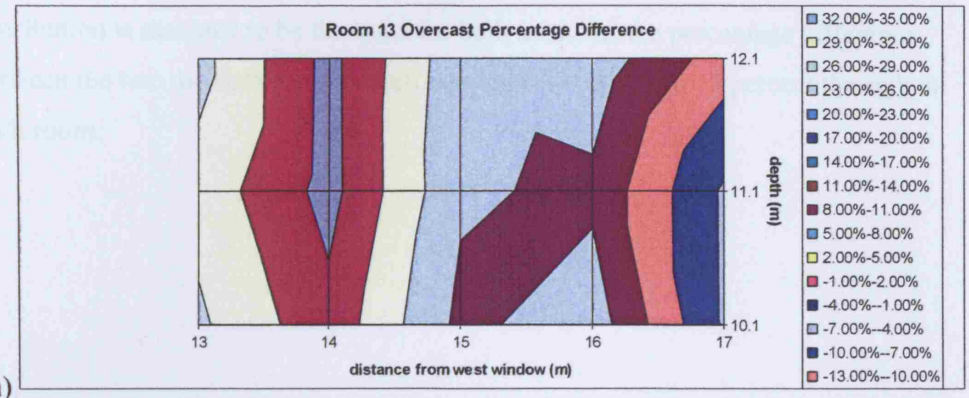

(n)

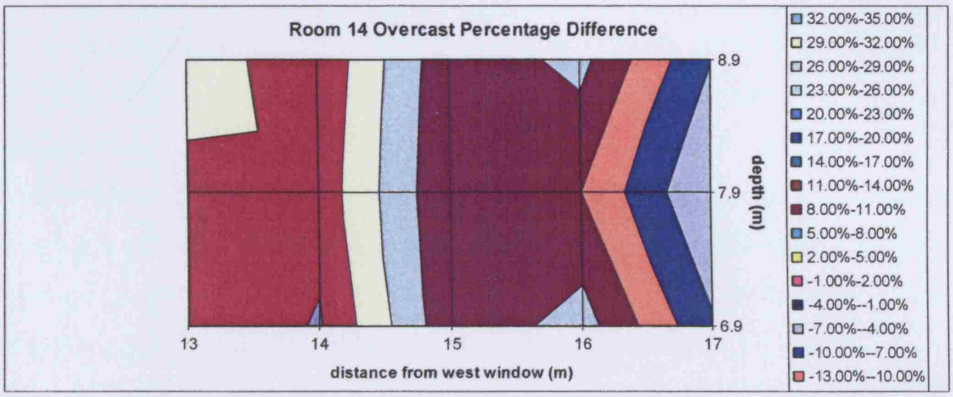

(o)

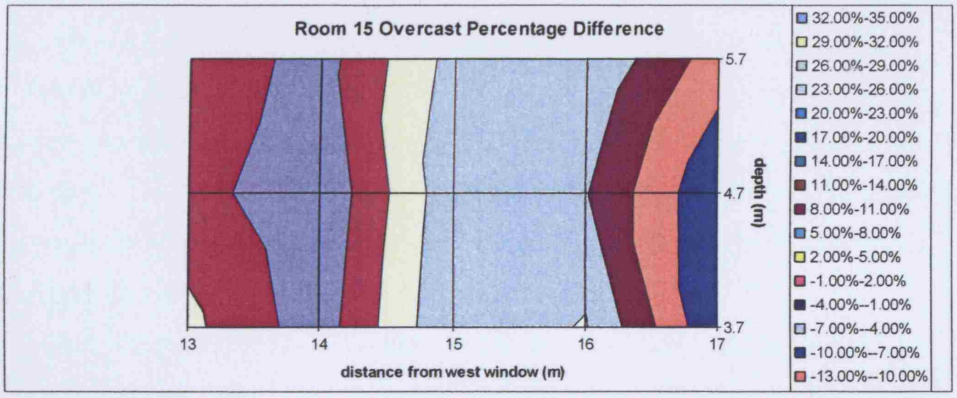

(p)

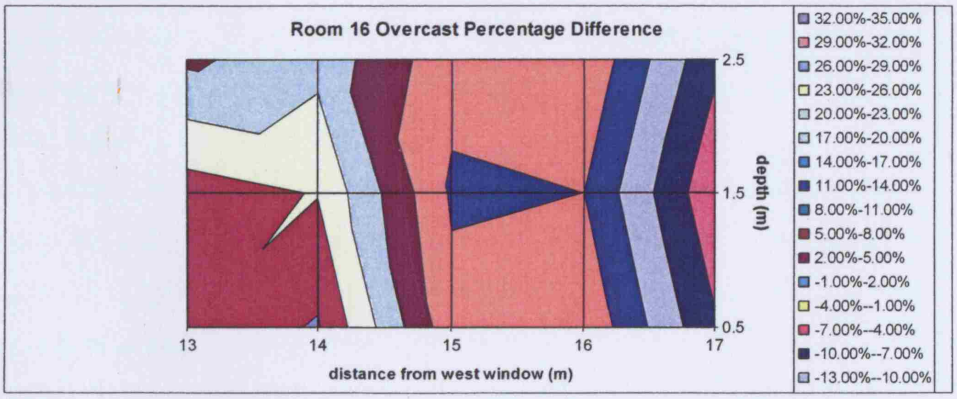

Figure 3.31 (m), (n), (o), (p): Room 13 to 16 overcast percentage difference

As can be seen from Figure 3.31, under an overcast sky, where the luminance distribution is assumed to be the same for both methods, the percentage difference between the two methods is very small ranging between 0 and 15 percent throughout each room.

Chapter 4

Conclusion

4.1 Summary

The goal of this paper was to determine whether the new method formulated by Peter J. Raynham based on the sunlight factor could accurately predict daylight illuminance. Raynham's method was compared against the daylight coefficient approach whose accuracy was verified by John Mardaljevic. In Chapter 3, a simple office space was modelled in *Radiance* and the illuminance was evaluated using both the daylight coefficient approach and the sunlight factor approach. It has been demonstrated that Raynham's method and that of Mardaljevic diverge in terms of their results, with the difference becoming much more significant further away from the windows. It can therefore be deduced that Raynham's method does not work.

Raynham's source of error is that he assumes an overcast sky to determine the diffuse component. But an overcast sky has a dark horizon and brighter zenith with ratio of about 1 to 3. Thus, his method puts a lot of light higher in the sky as opposed to the ground as is the case of a clear sky. This results in lower illuminance values from side windows and probably higher from sky lights.

Mardaljevic concluded, on the basis of one set of results, that the daylight coefficient approach can be used to compute the long-term daylight performance of buildings. However, it is worth mentioning his method's weaknesses which could become much more significant when the daylight coefficient approach is used for a different locale (as opposed to Garston, UK).

Mardaljevic subdivides the sky into many "circular" patches as opposed to "rectangular" patches specified by Tregenza and Waters. This is because at the moment it is not possible to specify a "rectangular" source angle in *Radiance* in a straightforward way. These "circular" patches do not, of course, offer complete sky coverage[11](Figure 4.1). As a result, the illuminance predicted at a point could potentially be underestimated.

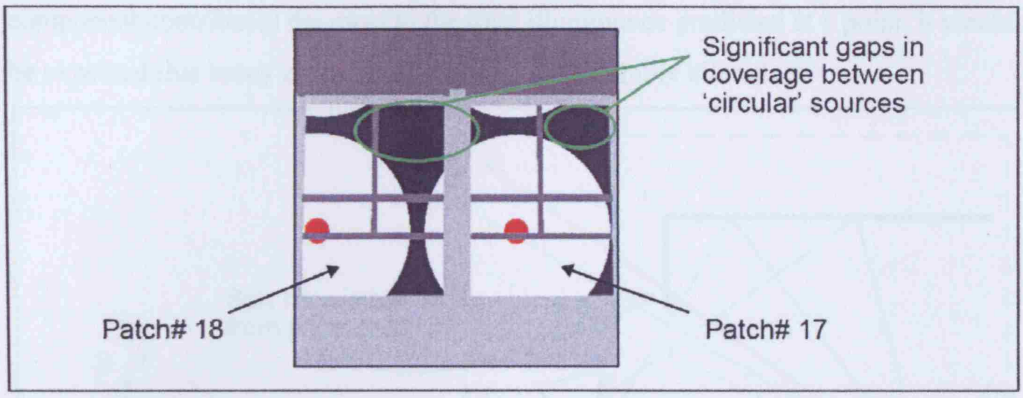

Figure 4.1: Incomplete sky coverage with "circular" sources

Another potential problem could also arise from the source angle type `light` used to model each luminous sky patch. This source angle is sampled with a single ray which is directed in the source centre (Figure 4.2). Hence, the daylight coefficient for each patch is calculated using rays that sample only the point at the patch centre. The result of single-ray light source sampling is that the contribution to direct illuminance is calculated on the basis of total source visibility, or total source occlusion. As a consequence, depending on the position of the calculation point, the direct sky component could be significantly overestimated, or even predicted to be zero[11].

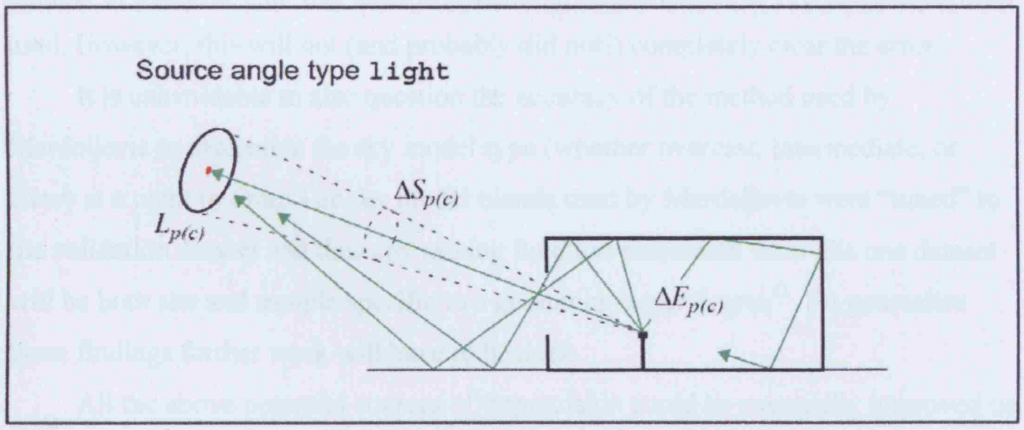

Figure 4.2: The formulation of each patch

In addition, significant errors may arise when the daylight coefficients are used to calculate the illumination from the sun (and thus the direct component). When the difference between the actual sun position and the centre of the nearest patch is large, there is a great possibility that a point will be evaluated to be in shade when it was actually illuminated in the sun – or vice-versa[11] (Figure 4.3). Given that the direct

component contributes the most to the total illuminance predicted at a point, it would be expected that many of the results will be considerably altered.

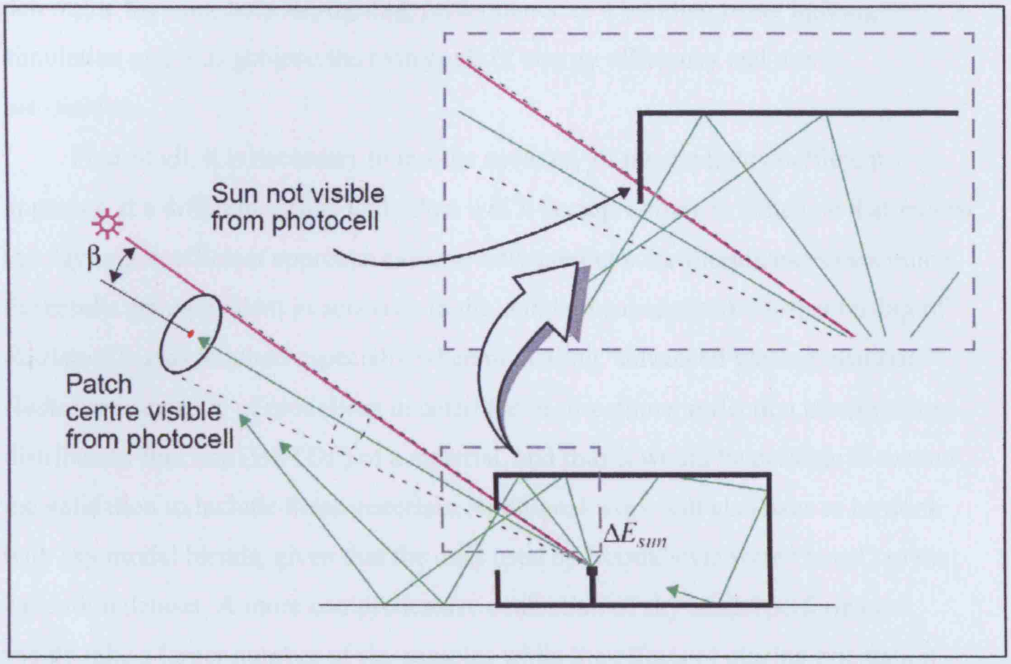

Figure 4.3: Sun displacement angle

It is possible to reduce these errors in Mardaljevic's method by using a larger number of sources. This was done in Chapter 3, where a total of 19,582 sources were used. However, this will not (and probably did not!) completely clear the error.

It is unavoidable to also question the accuracy of the method used by Mardaljevic to determine the sky model type (whether overcast, intermediate, or clear) at a point in time. The sky model blends used by Mardaljevic were "tuned" to the validation dataset and thus any mixing function elucidated from this one dataset will be both site and sample specific to a greater or lesser degree[11]. To generalise these findings further work will have to be done.

All the above potential sources of imprecision could be eventually improved on or fixed. There is one type of error, though, which at the moment has no scope for improvement. The finite resolution of the BRE sky scanner and solar tracker could result in deficiencies that limit the potential accuracy of the illuminance predictions. As a result, the direct component of illuminance resulting from the circumsolar region could be in error due to the uncertainty in the sky luminance distribution about the solar position.

4.2 Suggestions for future work

There is much more work that needs to be done in order to be able to accurately determine the long-term daylighting performance of a building using lighting simulation and thus achieve the twin goals of energy efficiency and user's satisfaction.

First of all, it is necessary to test the accuracy of the daylight coefficient approach at a different locale. Only then will it be appropriate to conclude that indeed the daylight coefficient approach can correctly predict solar illuminances (assuming the results are equivalent in accuracy to the standard calculation). Further testing of *Radiance* is also required especially when modelling "advanced glazing materials". *Radiance* is capable of modelling in detail the bi-directional reflection transmission distribution function (BRTDF) of a material, and thus it would be possible to extend the validation to include these materials. Additional work will also have to be done with sky model blends, given that the ones used by Mardaljevic were "tuned" to the validation dataset. A more comprehensive evaluation of sky model performance should take a larger number of sky samples while the effects of glazing orientation should also be examined.

The BRE-IDMP validation dataset has been extensively used to predict time varying daylight illumination for arbitrary sky and sun conditions. But given the increase in anthropogenic greenhouse gas concentrations, the global surface temperature is expected to increase by 1.1 to 6.4°C between 1990 and 2100[20]. To predict annual daylighting provision with any certainty therefore, it is necessary to synthesise a "statistically average" year even if several years data is required.

The presence of windows to allow daylight to enter a space and to allow occupants to look out has a major effect on both the energy efficiency of the building and human's wellbeing. Appropriate daylight systems are necessary to improve the distribution and penetration of daylight into a room, thus increasing the usefulness of daylight while keeping its harmful effects to a minimum. Lighting analysis became more sophisticated with the implementation of the daylight coefficient approach. However, further work is required not only to take into account the prevailing meteorological conditions but to also be certain that the potential sources of error of this method do not gross over or under-predict the internal illuminance.

Bibliography

1 Baker N, Steemers K. Daylight design of buildings, 2002.

2 British Standard: Lighting for buildings - Part 2: Code of Practice for daylighting, 1992.

3 BS ISO 15469: 2004 International Standard, Spatial distribution of daylight – CIE standard general sky.

4 Darula S, Kittler Richard. CIE General sky standard defining luminance distributions.

5 Daylighting and window design, *CIBSE Lighting Guide LG10:1999.*

6 Escuyer S, Fontoynont M, Lighting controls: a field study of office worker's reactions, *Lighting Research and Technology*, 32(2), 77-96, 2001.

7 Kambezidis H.D. Daylight climatology in the Athens urban environment: guidance for building designers, *Lighting Research and Technology*, 34,4, pp 297-312, 2001.

8 Larson W.L, Shakespeare R. Rendering with Radiance, 1997.

9 Littlefair P.J. Comparison of sky luminance models, *Solar Energy*, 53(4), 315-322, 1994.

10 Littlefair P.J. Predicting lighting energy use under daylight linked lighting controls, *Building Research and Information*, 26(4), 208-222, 1998.

11 Mardaljevic J. Daylight Simulations: Validation, Sky Models and Daylight Coefficients. PhD thesis. De Montfort, Leicester (UK): De Montfort University, Inst. Of Energy and Sustainable Development, 1999.

12 Mardaljevic J. Simulation of annual daylighting profiles for internal illuminance, *Lighting Research and Technology,* 32(3), 111-118, 2000.

13 Mardaljevic J. The BRE-IDMP dataset: a new benchmark for the validation of illuminance prediction techniques, *Lighting Research and Technology,* 33(2), 117-136, 2001.

14 Masters G.M, Renewable and efficient electric power systems, 2004.

15 Perez R, Ineichen P, Seals R, Modeling daylight availability and irradiance components from direct and global irradiance, *Solar Ennergy*, 44(5), 271-289, 1990.

16 Phillips D. Daylighting : natural light in architecture, 2004.

17 The IDMP Network, http://idmp.entpe.fr/

18 Tregenza P.R, Waters I.M. Daylight coefficients, *Lighting Research and Technology*, 15(2), 65-71, 1983.

19 van Bommel Ir.W.J.M, van den Beld Ir.G.J, Lighting for work: visual and biological effects, Philips Lighting, April 2003.

20 Wikipedia, the free encyclopedia, http://en.wikipedia.org/